International Journal of Solids and Structures 150 (2018) 241–254

Contents lists available at ScienceDirect

International Journal of Solids and Structures

journal homepage: www.elsevier.com/locate/ijsolstr

Surface effect in axisymmetric Hertzian contact problems

Ning Jia[b,d], Yin Yao[a,c], Zhilong Peng[a,c], Yazheng Yang[a,c], Shaohua Chen[a,c,*]

[a] Institute of Advanced Structure Technology, Beijing Institute of Technology, Beijing 100081, China
[b] LNM, Institute of Mechanics, Chinese Academy of Sciences, Beijing 100190, China
[c] Beijing Key Laboratory of Lightweight Multi-functional Composite Materials and Structures, Beijing Institute of Technology, Beijing 100081, China
[d] School of Engineering Sciences, University of Chinese Academy of Sciences, Beijing 100049, China

ARTICLE INFO

Article history:
Received 6 November 2017
Revised 31 May 2018
Available online 28 June 2018

Keywords:
Axisymmetric Hertzian contact
Surface effect
Surface energy density
Intrinsic length
Nano-indentation hardness

ABSTRACT

Surface effect in three different axisymmetric Hertzian contact models is investigated in this paper with a recently developed elastic theory for nanostructured materials, including a Boussinesq problem, contact problem between a rigid flat-ended cylindrical indenter and an elastic half space as well as contact problem between a rigid spherical indenter and an elastic half space. With the help of the Love's strain function method and Hankel integral transformation, closed-form solutions of the stress and displacement fields at the surface of an elastic half space subjected to a concentrated force are achieved, based on which the interface tractions and displacements in the three different axisymmetric contact problems can be further obtained. It is found that surface effect in these contact problems can be characterized only by an intrinsic length, i.e., the ratio of the bulk surface energy density to the bulk shear modulus of the indented material. When the contact radius is comparable with the intrinsic length, surface effect is much obvious, leading to a serious deviation between the two solutions predicted respectively by the theoretical model developed for nanomaterials and the classical contact model. A more interesting phenomenon is about surface effect on the indentation hardness, which is found to increase with the reduction of the indenter radius when the external load is fixed, or to increase with the decrease of the external load when the indenter radius keeps unchanged. All the results in this paper should be helpful not only for deep understanding of the surface effect on nano-contact behaviors but also for further revealing the nature of surface effect of nano-indentation hardness.

1. Introduction

Nano-materials, as an important and integral part in the development of nanoscience and nanotechnology, have been widely applied in many frontiers, for example, electrochemistry (Chan et al., 2007), stretchable electronics (Rogers et al., 2010) and nano-electro-mechanical systems (Poncharal et al., 1999), due to their excellent physical and mechanical properties as compared to bulk materials. Numerous experimental evidences have illustrated that many important properties, including the melting temperature (Qi and Wang, 2004), elastic modulus (Jing et al., 2006), resonant frequency (Cuenot et al., 2004), yield strength (Zhang et al., 2010) and indentation hardness (Gerberich et al., 1999; Wei et al., 2004), are size dependent when the characteristic length of materials or the indentation depth is on the order of nanoscale. Therefore, how to predict and explain the distinct size-dependent material properties becomes a key issue for the application of nanomaterials.

Size effect in nano-materials is essentially due to the large ratio of surface/interface to volume, which is also addressed as surface or interface effect (Gerberich et al., 2002; Zhang and Xu, 2002). From the atomic point of view, atoms at or near the free surface of a material would experience a discrepant local environment as compared to those in the bulk, which leads to an excess energy of each atom at or near the surface. When the characteristic length of a material shrinks to nanometers, the influence of the excess energy on the material properties would become significant. From the continuum viewpoint, the total excess energy can be described by the surface free energy and surface stress (Gibbs, 1906; Shuttleworth, 1950). Gurtin and Murdoch (1975,1978) formulated a rigorous surface elastic theory (G-M model) to account for the surface effect in nanomaterials, in which surface elastic constants are introduced due to the elastic surface constitutive relation. Such a model was then extensively studied. Dingreville et al. (2005) and Dingreville and Qu (2008) developed a framework incorporating the surface free energy, the interfacial excess energy and excess stress into the continuum theory.

* Corresponding author at: Institute of Advanced Structure Technology and Beijing Key Laboratory of Lightweight Multi-functional Composite Materials and Structures, Beijing Institute of Technology, Beijing 100081, China.
E-mail addresses: chenshaohua72@hotmail.com, shchen@bit.edu.cn (S. Chen).

https://doi.org/10.1016/j.ijsolstr.2018.06.019
0020-7683/

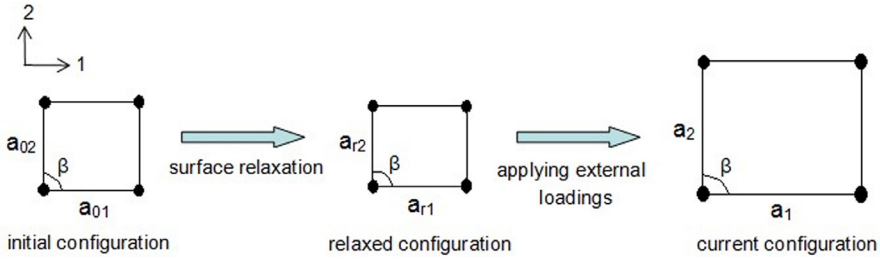

Fig. 1. Schematic of a surface unit cell and the corresponding lattice lengths in two principal directions in the initial (reference), relaxed and current configurations, respectively.

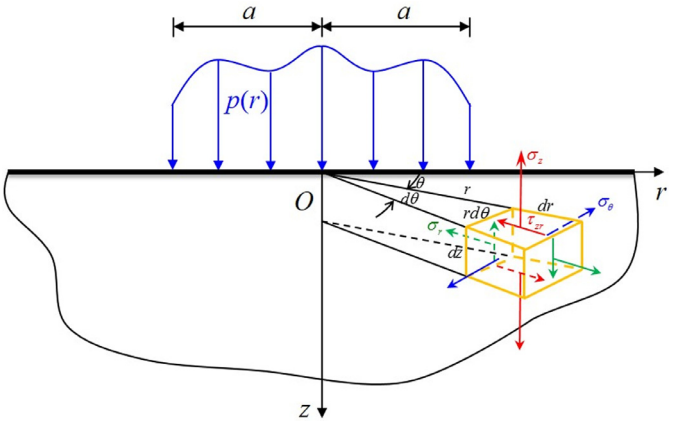

Fig. 2. Schematic of the axisymmetric contact model of an elastic half space subjected to an axisymmetric but non-uniform pressure $p(r)$ at a circular area of radius a.

Steigmann and Ogden (1997,1999) and Chhapadia et al. (2011) further investigated the influence of curvature-dependent surface energy on the effective elastic modulus of nanomaterials. Huang and Wang (2006,2010), Huang and Sun (2007) and Huang (2010) established a hyperelastic theoretical framework, in which the interface energy and the residual elastic field induced by the interface energy were taken into account. Both the curvature-dependent interface energy and the interface and bulk residual elastic fields were considered by Gao et al. (2014,2017).

The G-M theoretical framework and its extensions have been widely adopted to predict the size-dependent elastic properties of many nanostructured materials, from simple nanowires, nanofilms, nanoparticles to relatively complex nanocomposites and elastic media with nano-cracks (Cammarata, 1994; Streitz et al., 1994; Sharma et al., 2003; He et al., 2004; Duan et al., 2005; Wang and Feng, 2007b; He and Lilley, 2008; Wolfer, 2011; Huang and Wang, 2013; Nguyen et al., 2015; Nguyen et al., 2016; Takrori and Ayyad, 2017).

Recently, surface effect in contact mechanics attracts many interests, including the Boussinesq problem (Gao et al., 2013; Zhou and Gao, 2013), the Cerruti problem (Chen and Zhang, 2010; Zhou and Gao, 2014) and the plane strain or axisymmetric model of indenters with different shapes contacting an elastic substrate or a layer-substrate system (Long et al., 2012; Long and Wang, 2013; Pinyochotiwong et al., 2013; Zhou and Gao, 2013; Rungamornrat et al., 2016; Tirapat et al., 2017). Compared with the classical contact model (Johnson, 1987), additional surface-induced tractions as a function of surface stress are introduced at the contact surface, which depends not only on the surface residual stress resulted from surface relaxation but also on the surface deformation yielded by the external load, i.e., $\boldsymbol{\sigma}_s = \tau_0 \mathbf{I} + \mathbf{C}_s : \boldsymbol{\varepsilon}_s$. Here, $\boldsymbol{\sigma}_s$, τ_0, $\mathbf{I}$, $\mathbf{C}_s$ and $\boldsymbol{\varepsilon}_s$ denote the surface stress tensor, surface residual stress, unit tensor, surface elastic tensor and surface strain tensor, respectively.

From the way of surface treatment, the existing contact models can be categorized into three classes. In the first one, the surface stress equals to a constant surface residual stress and the effect of surface elasticity is neglected (Hajji, 1978; He and Lim, 2006; Wang and Feng, 2007a; Long et al., 2012; Long and Wang, 2013). In the second one, only the effect of surface elasticity is included without considering the surface residual stress induced by surface relaxation (Zhao and Rajapakse, 2009). In the last one, both effects of the surface residual stress and surface elasticity are involved (Koguchi, 2008; Chen and Zhang, 2010; Gao et al., 2013; Pinyochotiwong et al., 2013; Zhou and Gao, 2013; Zhou and Gao, 2014; Vasu and Bhandakkar, 2016). The common conclusion is that the normal traction and displacement at the contact surface would be mainly influenced by the surface residual stress, while the surface elasticity, as a dominant factor, would mainly affect the tangential traction at the contact surface.

Almost all the above contact models are based on G-M model or its extensions. Both values of the involved surface residual stress and surface elastic constants are difficult to determine. The former induced by surface relaxation is always assumed to be a constant, which should be influenced by the characteristic length of nanomaterials or nanostructures (Zhang et al., 2014). The latter is mainly determined with the help of molecular dynamics (MD) simulations (Miller and Shenoy, 2000; Shenoy, 2005; Mi et al., 2008). However, many factors would influence the numerical values, for example, the chosen atomic potential, size of the numerical model and the truncation of atom layers regarded as the surface of nanomaterials. Consequently, some questions still remain open: How can the surface elastic constants be accurately determined and what thickness should be chosen to describe the surface layer in MD simulations? Are the values of the surface constants sensitive to the scales of a nanomaterial in the atomistic model? And is the physical definition of elastic constants the same in MD simulations as in existing theoretical models?

In order to avoid the above thorny problems, Chen and Yao (2014) developed a new elastic theory for nanomaterials, which is based on the atomic lattice model (Nix and Gao, 1998). Surface energy density, as a typical parameter, is adopted to describe surface effect in nanomaterials. Both the effect of surface relaxation and that of the external load on the surface energy density of nanomaterials are included. Furthermore, the residual strain induced by surface relaxation and the strain yielded by the external load can be well defined based on the atomic lattice model, which would show influence on the surface energy density of nanomaterials. Surface effect induced tractions as a function of surface energy density directly affect the stress boundary conditions of nanomaterials, as compared with the classical elasticity theory. Only two kinds of material parameters are involved in the new theory to characterize the surface effect, i.e., the bulk surface energy density (surface energy density of the corresponding bulk material) and the surface relaxation parameter, both of which have clearly physical meanings and are easy to

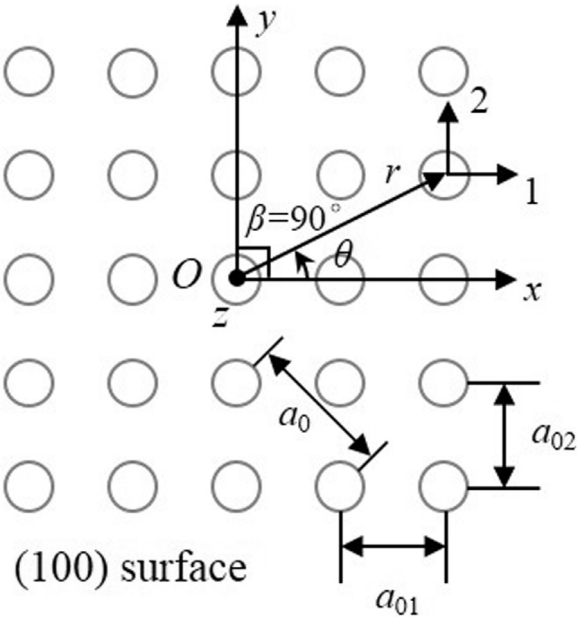

Fig. 3. The elastic fcc metallic half space with a (100) surface, where (1,2) denotes a local coordinate system on the surface and (r, θ, z) is a global cylindrical one.

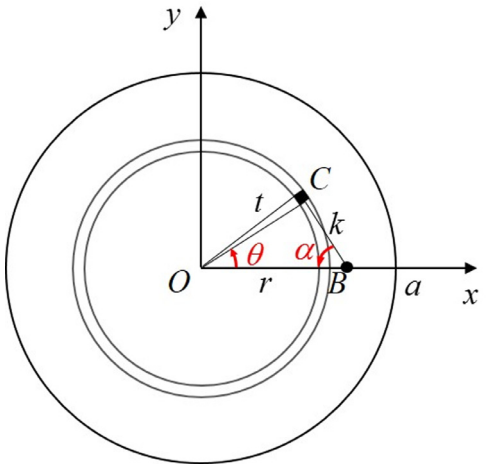

Fig. 4. Schematic of a circular loading area, where point B is an arbitrary one on the surface inside or outside the circular loading area and a concentrated force $p(t)td\theta dt$ acts on an infinitesimal surface element C.

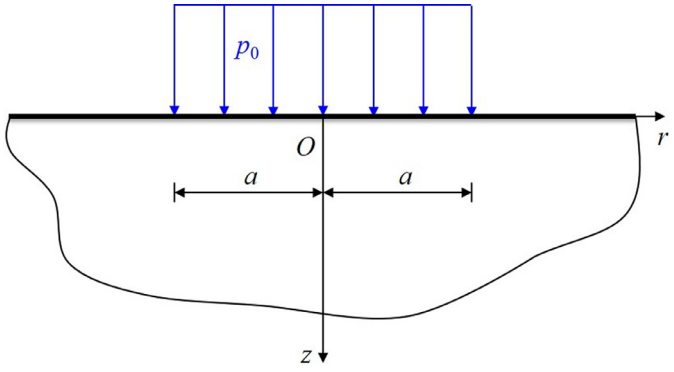

Fig. 5. The model of an elastic half space subjected to an axisymmetric and uniform pressure p_0 at an area of radius a.

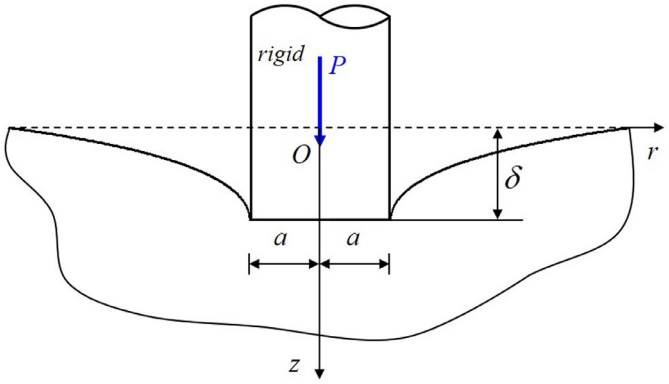

Fig. 6. The model a rigid flat-ended cylindrical indenter indenting an elastic half space, where the radius of the cylindrical indenter is a and δ is the indenting depth.

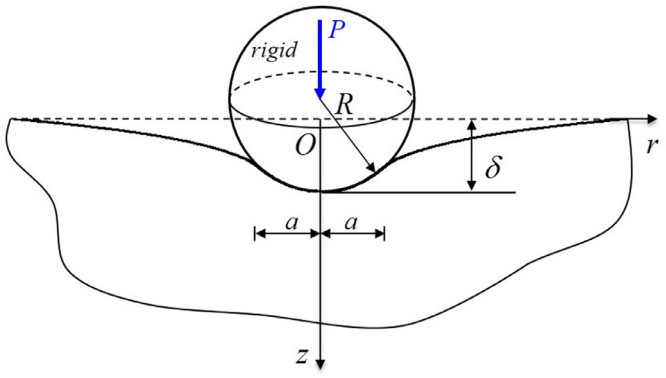

Fig. 7. The model a rigid spherical indenter indenting an elastic half space, where the radius of the spherical indenter is a and δ is the indenting depth.

find in material handbooks or simple MD simulations. Recently, a similar methodology is extended to investigate the interface effect in nanocomposites (Yao et al., 2017). Analysis of several typical problems has already verified the reasonability and feasibility of such a novel elastic theory, including surface effect in nanowires or nanobeams (Yao and Chen, 2015, 2016a,b; Jia et al., 2017b,c), nanoparticles (Yao et al., 2015), nanocomposites (Yao et al., 2017) and nano-indentation of plane strain contact problems (Jia et al., 2017a). Especially, with regard to the Hertzian contact problem considering surface effect, the normal pressure at the contact area would not obey the classically elliptical expressions any more (Johnson, 1987) due to the modified boundary conditions by the surface-induced tractions. Some work ignored such an issue (Gao et al., 2013; Zhou and Gao, 2013). More precise results have been achieved by Jia et al. (2017a) with the elastic theory developed by Chen and Yao (2014).

In this paper, the more realistic three-dimensional contact problem considering surface effect is investigated, in which three typical axisymmetric contact models are analyzed theoretically, including the Boussinesq problem, contact problem between a rigid flat-ended cylindrical indenter and an elastic half space as well as contact problem between a rigid spherical indenter and an elastic half space. Organization of the present paper is as follows. A brief introduction of the elastic theory using surface energy density to characterize surface effect of nanomaterials is given in Section 2. A generalized axisymmetric problem, i.e., an elastic half space subjected to an axisymmetric but non-uniform pressure, is analyzed in Section 3. Three typical axisymmetric contact problems are further analyzed respectively in Section 4. Results and discussion are given

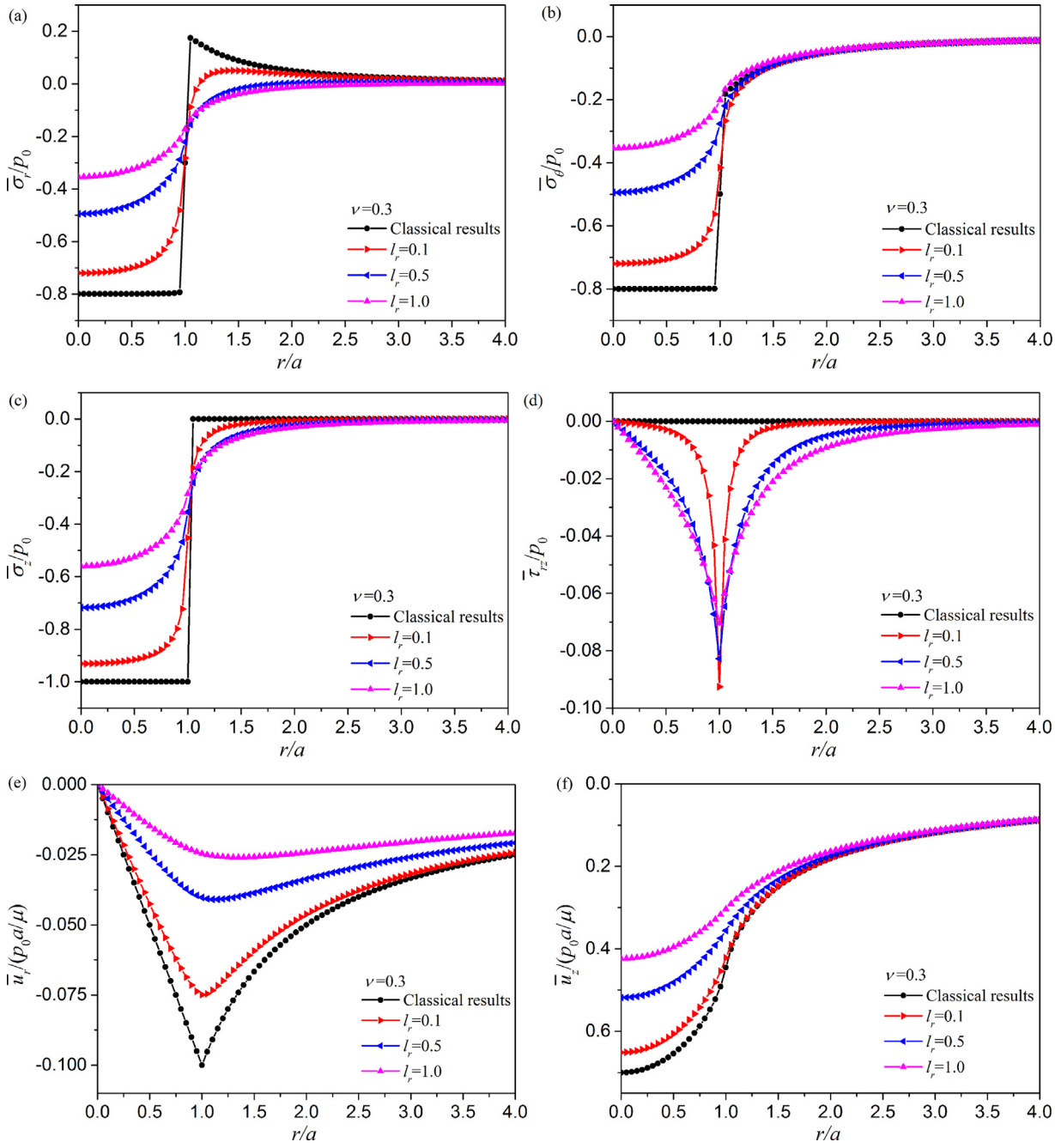

Fig. 8. Distributions of the stress and displacement at the contact surface in the model of an elastic half space subjected to a uniformly distributed pressure in a circular region. (a) For the non-dimensional radial stress $\bar{\sigma}_r$; (b) For the non-dimensional circumferential stress $\bar{\sigma}_\theta$; (c) For the non-dimensional normal stress $\bar{\sigma}_z$; (d) For the non-dimensional shear stress $\bar{\tau}_{rz}$; (e) For the non-dimensional radial displacement $\bar{u}_r$; (f) For the non-dimensional normal displacement $\bar{u}_z$.

in Section 5, where the classical contact results are also given for comparison and the size-dependent nano-indentation hardness is further discussed. Conclusions are made finally.

2. Brief introduction of the surface energy density-based elastic theory

Based on the atomic lattice model (Nix and Gao, 1998), an elastic theory for nanomaterials was proposed by Chen and Yao (2014), in which the surface effect is characterized by surface energy density.

The equilibrium equation and stress boundary conditions can be derived as

$$\begin{cases} \sigma \cdot \nabla + \mathbf{f} = 0 (\text{in} V - S) \\ \mathbf{n} \cdot \sigma \cdot \mathbf{n} = \mathbf{p} \cdot \mathbf{n} - \phi_0 (\mathbf{n} \cdot \nabla_s)/J_s (\text{on} S) \\ (\mathbf{I} - \mathbf{n} \otimes \mathbf{n}) \cdot \sigma \cdot \mathbf{n} = (\mathbf{I} - \mathbf{n} \otimes \mathbf{n}) \cdot \mathbf{p} + \phi_0 (\nabla_s J_s)/J_s^2 \\ \quad -(\nabla_s \phi_0)/J_s (\text{on} S) \end{cases} \tag{1}$$

where $\boldsymbol{\sigma}$ is the bulk Cauchy stress tensor inside the volume of the nano-solid V, ∇ denotes a spatial gradient operator in the current configuration of deformed nanomaterials, $\mathbf{n}$ is the unit normal vector perpendicular to the boundary surface S of the nano-solid and $\mathbf{I}$ is a unit tensor. $\boldsymbol{f}$ and $\boldsymbol{p}$ represent the body force and external surface traction, respectively. ϕ_0 denotes the Lagrangian surface en-

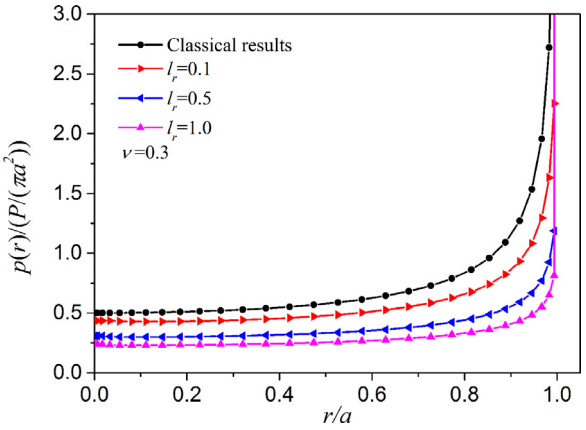

Fig. 9. Distribution of the non-dimensional contact pressure in the contact region of a rigid flat-ended cylindrical indenter indenting an elastic half space.

ergy density of nanomaterials. ∇_s is a surface gradient operator. J_s is a Jacobean determinant characterizing the surface deformation from a reference configuration to a current one.

Comparing to the classical elasticity theory, the stress boundary conditions in the elastic model for nanomaterials include the influence of the surface energy density, which is adopted to characterize the surface effect. The Lagrangian surface energy density ϕ_0 in the reference configuration can be further divided into two parts. One is a structural part ϕ_0^{stru} related to the surface strain energy induced by the residual strain leaded by surface relaxation and the surface strain yielded by the external loadings. The other is a chemical part ϕ_0^{chem} related to the surface dangling-bond energy induced by the unsaturated coordination.

$$\begin{aligned}
\phi_0 &= \phi_0^{stru} + \phi_0^{chem} \\
\phi_0^{stru} &= \frac{E_b}{2\sin\beta}\sum_{i=1}^{2} a_{0i}\eta_i\Big\{\Big[3+(\lambda_i+\lambda_i\varepsilon_{si})^{-m}-3(\lambda_i+\lambda_i\varepsilon_{si})\Big] \\
&\quad\times\Big[\lambda_i^2\varepsilon_{si}^2+(\lambda_i-1)^2+2\lambda_i(\lambda_i-1)\varepsilon_{si}\Big]\Big\} \\
\phi_0^{chem} &= \phi_{0b}\left(1-w_1\frac{D_0}{D}\right), \quad \eta_1=a_{01}/a_{02}, \quad \eta_2=a_{02}/a_{01}
\end{aligned} \tag{2}$$

where ϕ_{0b} is the bulk surface energy density, D_0 is a critical size ($D_0=3d_a$ for nanoparticles, nanowires and $2d_a$ for nanofilms, where d_a is the atomic diameter). D is a characteristic scale of nanostructured materials (e.g., thickness, diameter, etc.). w_1 is a parameter governing the size-dependent behavior of ϕ_0^{chem}. E_b is the bulk Young's modulus. a_{01}, a_{02} represent the initial lattice lengths of surface atoms in the two principal directions, respectively. β denotes an angle between the two basic vectors as shown in Fig. 1. The lattice lengths become a_{r1} and a_{r2} after spontaneous surface relaxation, and subsequently become a_1 and a_2 in the current configuration when subjected to an external loading. $\lambda_i=a_{ri}/a_{0i}$ denotes the surface relaxation parameter, $\varepsilon_{si}=(a_i-a_{ri})/a_{ri}$ is the surface strain induced only by the external loading and m is a parameter describing the dependence of bond lengths on the binding energy ($m=4$ for alloys or compounds and $m=1$ for pure metals). Details can be found in Chen and Yao (2014).

It can be found that only two material parameters, i.e., the bulk surface energy density ϕ_{0b} and the surface relaxation parameter λ_i, are involved to characterize the surface effect, both of which have clearly physical meanings and are very easy to find through Material Handbooks and simple MD simulations.

3. An elastic half space subjected to an axisymmetrically non-uniform pressure

As a fundamental model in contact mechanics (Johnson, 1987), the Boussinesq problem with surface effect is considered firstly. An axisymmetric but non-uniform pressure $p(r)$ is added on the surface of the elastic half space as shown in Fig. 2. A cylindrical coordinate system (r, θ, z) with origin O at the center of the loading area is attached on the surface, where r-axis is along the initially flat surface and z-axis is perpendicular to the surface. a denotes the radius of loading area. Surfaces beyond the loading area are traction-free.

3.1. Governing equations and boundary conditions

In the absence of a body force, the equilibrium equation of the axisymmetric indenting problem shown in Fig. 2 can be written as

$$\frac{\partial\sigma_r}{\partial r}+\frac{\partial\tau_{zr}}{\partial z}+\frac{\sigma_r-\sigma_\theta}{r}=0,\ \frac{\partial\tau_{rz}}{\partial r}+\frac{\partial\sigma_z}{\partial z}+\frac{\tau_{rz}}{r}=0 \tag{3}$$

where σ_r, σ_θ, σ_z denote the radial, circumferential and normal stresses, respectively. τ_{rz} is the only non-zero shear stress component.

With an assumption of infinitesimal deformation, the non-zero strain components, including the radial, circumferential and normal strains ε_r, ε_θ, ε_z, and the shear strain γ_{rz} can be expressed as

$$\varepsilon_r=\frac{\partial u_r}{\partial r},\ \varepsilon_\theta=\frac{u_r}{r},\ \varepsilon_z=\frac{\partial u_z}{\partial z},\ \gamma_{rz}=\frac{\partial u_r}{\partial z}+\frac{\partial u_z}{\partial r} \tag{4}$$

where u_r and u_z are the radial and normal displacements, respectively.

The elastic half space is assumed to abide by the linear Hooke's law,

$$\begin{aligned}
\sigma_r &= 2\mu\left[\frac{\nu}{1-2\nu}(\varepsilon_r+\varepsilon_\theta+\varepsilon_z)+\varepsilon_r\right], \\
\sigma_\theta &= 2\mu\left[\frac{\nu}{1-2\nu}(\varepsilon_r+\varepsilon_\theta+\varepsilon_z)+\varepsilon_\theta\right], \\
\sigma_z &= 2\mu\left[\frac{\nu}{1-2\nu}(\varepsilon_r+\varepsilon_\theta+\varepsilon_z)+\varepsilon_z\right],\ \tau_{zr}=\mu\gamma_{zr}
\end{aligned} \tag{5}$$

where μ and ν are the bulk shear modulus and Poisson's ratio of the elastic half space, respectively.

Different from the classical contact theory (Johnson, 1987), additional tractions would be induced by the surface effect besides the external normal pressure $p(r)$ (Chen and Yao, 2014). Thus, the stress boundary conditions at $z=0$ can be expressed as,

$$\begin{cases}\sigma_z|_{z=0}+p(r)=-\gamma_n \\ \tau_{rz}|_{z=0}=\gamma_r\end{cases} \tag{6}$$

where γ_n and γ_r denote the normal and radial surface-induced tractions, respectively.

According to Chen and Yao (2014), we have

$$\gamma_n=\frac{\phi_0}{J_s}\left(\frac{\partial^2 u_z}{\partial r^2}+\frac{1}{r}\frac{\partial u_z}{\partial r}\right)\Big|_{z=0},\ \gamma_r=\frac{1}{J_s}\frac{\partial\phi_0}{\partial r}-\frac{\phi_0}{J_s^2}\frac{\partial J_s}{\partial r}\Big|_{z=0} \tag{7}$$

For simplicity, the initial configuration of the elastic half space is assumed to be an un-deformed fcc metallic substrate with (100) surface as shown in Fig. 3, where a local coordinate system (1, 2) coincides with a global Cartesian one (x, y, z). As a result, in the structural part ϕ_0^{stru} of the Lagrangian surface energy density ϕ_0, we have $m=1$, $\beta=90°$ and an equal atomic spacing in both bond directions, i.e., $a_{01}=a_{02}=\sqrt{2}a_0/2$, where a_0 denotes the lattice constant of the bulk material. The surface relaxation in both bond directions would be neglected for an elastic half space, i.e., $\lambda_1=\lambda_2\approx 1$ (Zhang and Xu, 2002).

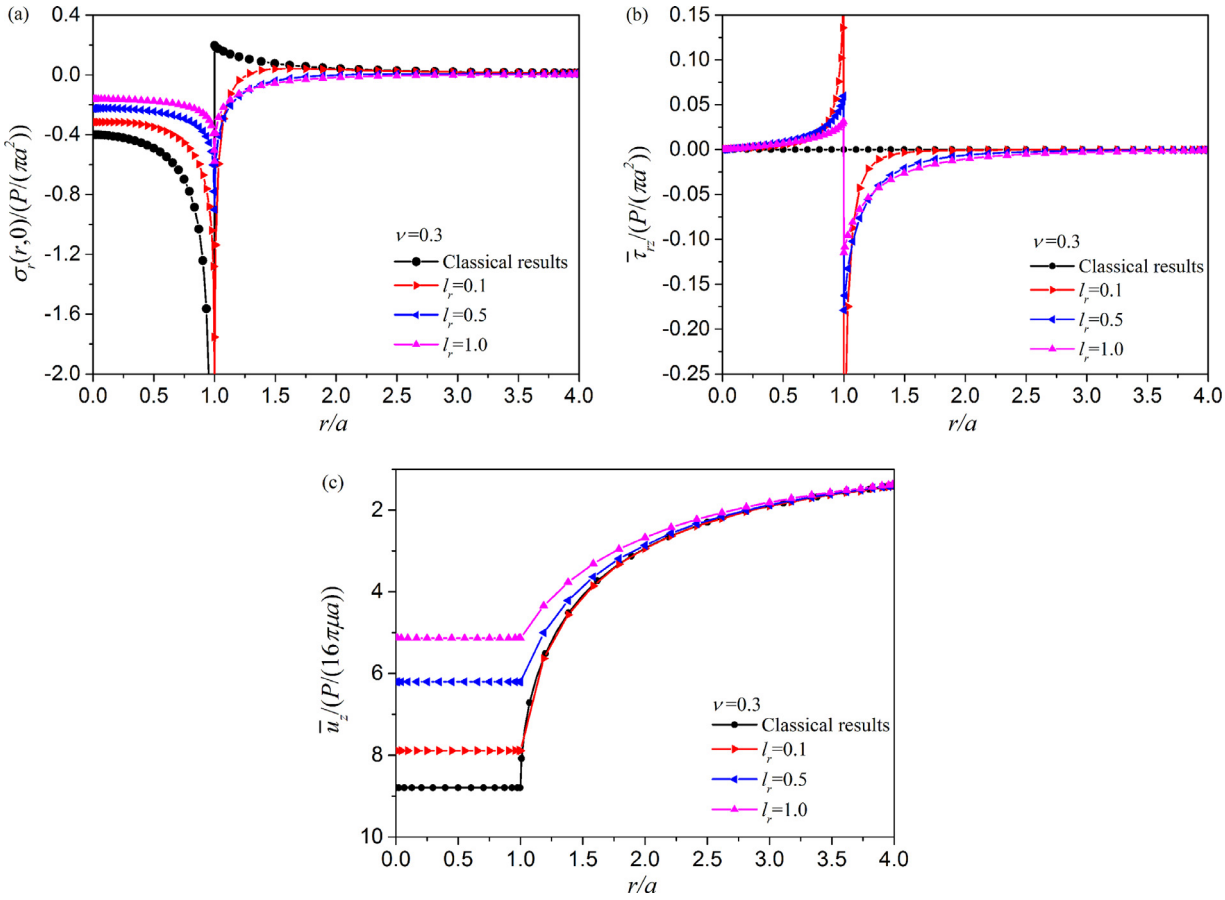

Fig. 10. Distributions of the stress and displacement at the contact surface in the model of a rigid flat-ended cylindrical indenter indenting an elastic half space. (a) For the non-dimensional normal stress $\bar{\sigma}_z$; (b) For the non-dimensional shear stress $\bar{\tau}_{rz}$; (c) For the non-dimensional normal displacement $\bar{u}_z$.

According to the relationship between the local coordinate system (1, 2) and the global cylindrical one (r, θ, z) as shown in Fig. 3, the surface strain ε_{si} ($i=1, 2$) in two bond directions can be obtained as $\varepsilon_{s1}=[(\varepsilon_r+\varepsilon_\theta)+(\varepsilon_r-\varepsilon_\theta)\cos 2\theta]/2|_{z=0}$ and $\varepsilon_{s2}=[(\varepsilon_r+\varepsilon_\theta)-(\varepsilon_r-\varepsilon_\theta)\cos 2\theta]/2|_{z=0}$ (Timoshenko and Goodier, 1951). The chemical part ϕ_0^{chem} of the Lagrangian surface energy density ϕ_0 should equal to the bulk surface energy density ϕ_{0b} due to the large characteristic length D, i.e., $\phi_0^{chem}=\phi_{0b}$. Thus, the Lagrangian surface energy density ϕ_0 of an elastic half space can be expressed as

$$\phi_0 \approx \phi_{0b}+\frac{\sqrt{2}E_b a_0}{8}\left[(\varepsilon_r+\varepsilon_\theta)^2+(\varepsilon_r-\varepsilon_\theta)^2\cos^2(2\theta)\right]\Big|_{z=0} \tag{8}$$

For an axisymmetric model, we approximately have

$$\phi_0 \approx \phi_{0b}+\frac{\sqrt{2}E_b a_0}{4}\left(\varepsilon_r^2+\varepsilon_\theta^2\right)\Big|_{z=0} \tag{9}$$

Combining Eqs. (7), (9) and noting that $J_s=1+\varepsilon_r+\varepsilon_\theta$, the stress boundary conditions in Eq. (6) can be rewritten as

$$\begin{cases} \sigma_z|_{z=0}+p(r)=-\phi_{0b}(1-\varepsilon_r-\varepsilon_\theta)\left(\dfrac{\partial^2 u_z}{\partial r^2}+\dfrac{1}{r}\dfrac{\partial u_z}{\partial r}\right)\Big|_{z=0} \\ \tau_{rz}|_{z=0}=-\phi_{0b}\Big[(1-\chi\varepsilon_r-2\varepsilon_\theta)\dfrac{\partial^2 u_r}{\partial r^2} \\ \quad +(1-\chi\varepsilon_\theta-2\varepsilon_r)\left(\dfrac{1}{r}\dfrac{\partial u_r}{\partial r}-\dfrac{u_r}{r^2}\right)\Big]\Big|_{z=0} \end{cases} \tag{10}$$

where $\chi=\sqrt{2}E_b a_0/(8\phi_{0b})+2$ is a dimensionless parameter related to the material properties. Under an infinitesimal deformation condition, the radial and circumferential strains ε_r and ε_θ are much less than 1. It suggests that the high-order terms in Eq. (10), e.g., the product of strain components with the partial derivatives of u_r, can be reasonable neglected. Moreover, when the surface effect is considered, the strain components should be significantly smaller than the classical counterparts (Gao et al., 2013; Long and Wang, 2013), while the latter ones are already very small quantities (much less than 0.1) when the substrate is only subjected to a normal pressure $p(r)$ (Johnson, 1987). Therefore, ε_r and ε_θ are negligible and the stress boundary conditions in Eq. (10) can be rewritten as

$$\begin{cases} \sigma_z|_{z=0}+p(r)=-\phi_{0b}\left(\frac{\partial^2 u_z}{\partial r^2}+\frac{1}{r}\frac{\partial u_z}{\partial r}\right)\Big|_{z=0} \\ \tau_{rz}|_{z=0}=-\phi_{0b}\left(\frac{\partial^2 u_r}{\partial r^2}+\frac{1}{r}\frac{\partial u_r}{\partial r}-\frac{u_r}{r^2}\right)\Big|_{z=0} \end{cases} \tag{11}$$

Compared with the classical contact theory (Johnson, 1987), the stress boundary conditions with surface effect depend significantly on the surface energy density of the indented bulk substrate ϕ_{0b}, which, as a dominant parameter, characterizes the surface property of an elastic half space in nano-contact models. The material parameter χ related to the bulk Young's modulus E_b and the lattice constant of the bulk material a_0 is neglected with the high-order terms.

Thus, the governing equations for such an axisymmetric boundary value problem considering surface effect are completely formulated in Eqs. (3)–(5) with boundary conditions in Eq. (11).

3.2. General solutions

Similar to the classical axisymmetric contact problem (Selvadurai, 2000), a scalar Love's strain function denoted by

$\Psi(r, z)$ is introduced, which should satisfy the biharmonic equation $\tilde{\nabla}^2\tilde{\nabla}^2\Psi(r,z)=0$ in the absence of body forces. Here, we have $\tilde{\nabla}^2=\partial^2/\partial r^2+(\partial/\partial r)/r+\partial^2/\partial z^2$ in the cylindrical coordinate system. Using Hankel integral transform method with respect to r, the stress and displacement components can be expressed as a function of the 0th-order Hankel transform of Love's strain function $\tilde{\Psi}(\xi,z)$,

$$\begin{cases}\sigma_r(r,z)=\int_0^\infty \xi\left[\nu\dfrac{\partial^3\tilde{\Psi}}{\partial z^3}+(1-\nu)\xi^2\dfrac{\partial\tilde{\Psi}}{\partial z}\right]J_0(\xi r)d\xi\\ \quad -\int_0^\infty \xi^2\dfrac{1}{r}\dfrac{\partial\tilde{\Psi}}{\partial z}J_1(\xi r)d\xi\\ \sigma_\theta(r,z)=\int_0^\infty \xi\nu\left[\dfrac{\partial^3\tilde{\Psi}}{\partial z^3}-\xi^2\dfrac{\partial\tilde{\Psi}}{\partial z}\right]J_0(\xi r)d\xi\\ \quad +\int_0^\infty \xi^2\dfrac{1}{r}\dfrac{\partial\tilde{\Psi}}{\partial z}J_1(\xi r)d\xi\\ \sigma_z(r,z)=\int_0^\infty \xi\left[(1-\nu)\dfrac{\partial^3\tilde{\Psi}}{\partial z^3}-(2-\nu)\xi^2\dfrac{\partial\tilde{\Psi}}{\partial z}\right]J_0(\xi r)d\xi\\ \tau_{rz}(r,z)=\int_0^\infty \xi^2\left[\nu\dfrac{\partial^2\tilde{\Psi}}{\partial z^2}+(1-\nu)\xi^2\tilde{\Psi}\right]J_1(\xi r)d\xi\end{cases} \tag{12}$$

and

$$\begin{cases}u_r(r,z)=\dfrac{1}{2\mu}\int_0^\infty \xi^2\frac{\partial\tilde{\Psi}}{\partial z}J_1(\xi r)d\xi\\ u_z(r,z)=\frac{1}{2\mu}\int_0^\infty \xi\left[(1-2\nu)\frac{\partial^2\tilde{\Psi}}{\partial z^2}-2(1-\nu)\xi^2\tilde{\Psi}\right]J_0(\xi r)d\xi\end{cases} \tag{13}$$

where $J_n(\xi r)$ denotes the nth Bessel function of the first kind. $\tilde{\Psi}(\xi,z)$ satisfies the following form

$$\tilde{\Psi}(\xi,z)=(A+Bz)e^{-\xi z} \tag{14}$$

where A and B can be determined by the stress boundary conditions.

Substituting Eq. (14) into Eqs. (12),(13), and then further into Eq. (11) yields

$$\begin{cases}A=-\dfrac{2(l\xi+4\nu)}{\xi^3(l\xi+2)[(3-4\nu)l\xi+2]}\tilde{p}(\xi)\\ B=-\dfrac{2(l\xi+2)}{\xi^2(l\xi+2)[(3-4\nu)l\xi+2]}\tilde{p}(\xi)\end{cases} \tag{15}$$

where $\tilde{p}(\xi)$ denotes the 0th Hankel transformation of $p(r)$ and is expressed as

$$\tilde{p}(\xi)=\int_0^\infty t\,p(t)J_0(\xi t)dt \tag{16}$$

The parameter l in Eq. (15) is an intrinsic length characterizing surface effect, which equals to the ratio of the bulk surface energy density to the bulk shear modulus,

$$l=\frac{\phi_{0b}}{\mu} \tag{17}$$

It is interesting to find that the intrinsic length in such an axisymmetric model possesses the same expression as that in a plane-strain contact problem with surface effect (Jia et al., 2017a). In contrast to the work based on the G-M model (Gao et al., 2013; Pinyochotiwong et al., 2013; Zhou and Gao, 2013), only one intrinsic length characterizing the surface effect is involved in the present analysis.

Substituting Eqs. (14) and (15) into Eq. (13) yields the stress and displacement components

$$\begin{cases}\sigma_r=-\int_0^\infty\dfrac{\xi[4(\nu l\xi+1)-2(l\xi+2)\xi z]}{(l\xi+2)[(3-4\nu)l\xi+2]}\tilde{p}(\xi)e^{-\xi z}J_0(\xi r)d\xi\\ +\dfrac{1}{r}\int_0^\infty\dfrac{4(1-2\nu)-2(l\xi+2)\xi z}{(l\xi+2)[(3-4\nu)l\xi+2]}\tilde{p}(\xi)e^{-\xi z}J_1(\xi r)d\xi\\ \sigma_\theta=-\int_0^\infty\dfrac{4\xi\nu(l\xi+2)}{(l\xi+2)[(3-4\nu)l\xi+2]}\tilde{p}(\xi)e^{-\xi z}J_0(\xi r)d\xi\\ -\dfrac{1}{r}\int_0^\infty\dfrac{2[2(1-2\nu)-(l\xi+2)\xi z]}{(l\xi+2)[(3-4\nu)l\xi+2]}\tilde{p}(\xi)e^{-\xi z}J_1(\xi r)d\xi\\ \sigma_z=-\int_0^\infty\dfrac{\xi[4(1-\nu)l\xi+4+2(l\xi+2)\xi z]}{(l\xi+2)[(3-4\nu)l\xi+2]}\tilde{p}(\xi)e^{-\xi z}J_0(\xi r)d\xi\\ \tau_{rz}=-\int_0^\infty\dfrac{\xi[2(1-2\nu)l\xi+2(l\xi+2)\xi z]}{(l\xi+2)[(3-4\nu)l\xi+2]}\tilde{p}(\xi)e^{-\xi z}J_1(\xi r)d\xi\end{cases} \tag{18}$$

and

$$\begin{cases}u_r=-\dfrac{1}{2\mu}\int_0^\infty\dfrac{2[2(1-2\nu)-(l\xi+2)\xi z]}{(l\xi+2)[(3-4\nu)l\xi+2]}\tilde{p}(\xi)e^{-\xi z}J_1(\xi r)d\xi\\ u_z=\dfrac{1}{2\mu}\int_0^\infty\dfrac{2[(3-4\nu)l\xi+4(1-\nu)+(l\xi+2)\xi z]}{(l\xi+2)[(3-4\nu)l\xi+2]}\\ \quad\tilde{p}(\xi)e^{-\xi z}J_0(\xi r)d\xi\end{cases} \tag{19}$$

where the solutions tend to the classical ones (Johnson, 1987; Selvadurai, 2000) when the parameter l become zero.

In order to facilitate the calculation, we further transform the infinite integral into an easy-solving form with a finite integral. Assume that the half space is subjected to a unit concentrated vertical force $p(r)=\delta(r)$ at the origin O. Then, Eq. (16) yields $\tilde{p}(\xi)=1/(2\pi)$. Using the knowledge of Bessel integral Abramowitz and Stegun, 1964) and Eqs. (18) and (19), the stress and displacement fields at the surface (at $z=0$) in the model of an elastic half space subjected to a unit concentrated force can be achieved as,

$$\begin{cases}\bar{\sigma}_r^{uc}=-\dfrac{1}{2\pi l^2}\left[\dfrac{4\nu l}{(3-4\nu)r}+2\Xi_{01}(r)-\dfrac{6\Xi_{02}(r)}{(3-4\nu)^2}\right]\\ \quad+\dfrac{-\Xi_{11}(r)+\Xi_{12}(r)}{2\pi lr}\\ \bar{\sigma}_\theta^{uc}=-\dfrac{1}{2\pi l^2}\left[\dfrac{4\nu l}{(3-4\nu)r}-\dfrac{8\nu\Xi_{02}(r)}{(3-4\nu)^2}\right]-\dfrac{-\Xi_{11}(r)+\Xi_{12}(r)}{2\pi lr}\quad\text{at } z=0\\ \bar{\sigma}_z^{uc}=-\dfrac{1}{2\pi l^2}\left[\dfrac{4(1-\nu)l}{(3-4\nu)r}-2\Xi_{01}(r)-\dfrac{2\Xi_{02}(r)}{(3-4\nu)^2}\right]\\ \bar{\tau}_{rz}^{uc}=-\dfrac{1}{2\pi l^2}\left[\dfrac{2(1-2\nu)l}{(3-4\nu)r}-2\Xi_{11}(r)+\dfrac{2\Xi_{12}(r)}{(3-4\nu)^2}\right]\end{cases} \tag{20}$$

and

$$\begin{cases}\bar{u}_r^{uc}=-\dfrac{1}{4\pi\mu l}[-\Xi_{11}(r)+\Xi_{12}(r)]\\ \bar{u}_z^{uc}=\dfrac{1}{4\mu\pi l}[\Xi_{01}(r)+\Xi_{02}(r)]\end{cases}\quad\text{at } z=0 \tag{21}$$

where the superscript "uc" denotes "unit concentrated". The bar "-" emphasizes the solution at $z=0$. Meanwhile,

$$\Xi_{\hat{m}\hat{s}}(r)=\begin{cases}\dfrac{\pi}{2}\left[H_0\left(\dfrac{b_{\hat{s}}r}{l}\right)-Y_0\left(\dfrac{b_{\hat{s}}r}{l}\right)\right](\hat{m}=0)\\ \dfrac{l}{b_{\hat{s}}r}+1-\dfrac{\pi}{2}\left[H_1\left(\dfrac{b_{\hat{s}}r}{l}\right)-Y_1\left(\dfrac{b_{\hat{s}}r}{l}\right)\right](\hat{m}=1)\end{cases} \tag{22}$$

$\hat{s}=1\text{ or }2,\ b_1=2,\ b_2=2/(3-4\nu)$

Here, H_n and Y_n are the nth Struve function and the nth Bessel function of the second kind, respectively.

When the elastic half space is subjected to an axisymmetric but non-uniform pressure $p(r)$, the stress and displacement fields at any point B on the surface inside or outside the circular loading area could be obtained by double integral of the result produced

by a concentrated force $p(t)td\theta dt$ acting on an infinitesimal surface element C as shown in Fig. 4,

$$\begin{cases} \bar{\sigma}_r = \frac{1}{2}\int_0^a\int_0^{2\pi}\left\{\begin{array}{l}\bar{\sigma}_r^{uc}(k,0)+\bar{\sigma}_\theta^{uc}(k,0)\\ +\left[\bar{\sigma}_r^{uc}(k,0)-\bar{\sigma}_\theta^{uc}(k,0)\right]\left(2\cos^2\alpha-1\right)\end{array}\right\} \\ \quad p(t)td\theta dt \\ \bar{\sigma}_\theta = \frac{1}{2}\int_0^a\int_0^{2\pi}\left\{\begin{array}{l}\bar{\sigma}_\theta^{uc}(k,0)+\bar{\sigma}_r^{uc}(k,0)\\ +\left[\bar{\sigma}_\theta^{uc}(k,0)-\bar{\sigma}_r^{uc}(k,0)\right]\left(2\cos^2\alpha-1\right)\end{array}\right\} \\ \quad p(t)td\theta dt \\ \bar{\sigma}_z = \int_0^a\int_0^{2\pi}\bar{\sigma}_z^{uc}(k,0)p(t)td\theta dt \\ \bar{\tau}_{rz} = -\int_0^a\int_0^{2\pi}\bar{\tau}_{rz}^{uc}(k,0)\cos\alpha\, p(t)td\theta dt \end{cases} \tag{23}$$

and

$$\begin{cases} \bar{u}_r = -\int_0^a\int_0^{2\pi}\bar{u}_r^{uc}(k,0)\cos\alpha\, p(t)td\theta dt \\ \bar{u}_z = \int_0^a\int_0^{2\pi}\bar{u}_z^{uc}(k,0)p(t)td\theta dt \end{cases} \tag{24}$$

where $k=\sqrt{r^2+t^2-2rt\cos\theta}$ and $\cos\alpha=(r-t\cos\theta)/k$.

Let $t=a(t'+1)/2$, $r=a(r'+1)/2$, $l=l_r a$ and $k=k_r a/2$. Eqs. (23) and (24) can be rewritten as,

$$\begin{cases} \bar{\sigma}_r = \frac{1}{16\pi l_r}\int_{-1}^1\int_0^{2\pi}\left[(f_1+f_2)+(f_1-f_2)\left(2\cos^2\alpha-1\right)\right] \\ \quad \left(t'+1\right)p\left[\frac{a}{2}\left(t'+1\right)\right]d\theta dt' \\ \bar{\sigma}_\theta = \frac{1}{16\pi l_r}\int_{-1}^1\int_0^{2\pi}\left[(f_2+f_1)+(f_2-f_1)\left(2\cos^2\alpha-1\right)\right] \\ \quad \left(t'+1\right)p\left[\frac{a}{2}\left(t'+1\right)\right]d\theta dt' \\ \bar{\sigma}_z = -\frac{1}{8\pi l_r^2}\int_{-1}^1\int_0^{2\pi}\left[\frac{8(1-\nu)l_r}{(3-4\nu)k_r}-2\Xi'_{01}(k_r)-\frac{2\Xi'_{02}(k_r)}{(3-4\nu)^2}\right] \\ \quad \left(t'+1\right)p\left[\frac{a}{2}\left(t'+1\right)\right]d\theta dt' \\ \bar{\tau}_{rz} = -\frac{1}{8\pi l_r^2}\int_{-1}^1\int_0^{2\pi}\left[\begin{array}{l}\frac{4(1-2\nu)l_r}{(3-4\nu)k_r}-2\Xi'_{11}(k_r)\\ +\frac{2\Xi'_{12}(k_r)}{(3-4\nu)^2}\end{array}\right] \\ \quad \cos\alpha\left(t'+1\right)p\left[\frac{a}{2}\left(t'+1\right)\right]d\theta dt' \end{cases} \tag{25}$$

and

$$\begin{cases} \bar{u}_r = -\frac{a}{16\pi\mu l_r}\int_{-1}^1\int_0^{2\pi}\left[-\Xi'_{11}(k_r)+\Xi'_{12}(k_r)\right] \\ \quad \cos\alpha\left(t'+1\right)p\left[\frac{a}{2}\left(t'+1\right)\right]d\theta dt' \\ \bar{u}_z = \frac{a}{16\mu\pi l_r}\int_{-1}^1\int_0^{2\pi}\left[\Xi'_{01}(k_r)+\Xi'_{02}(k_r)\right]\left(t'+1\right) \\ \quad p\left[\frac{a}{2}\left(t'+1\right)\right]d\theta dt' \end{cases} \tag{26}$$

where

$$\begin{aligned} f_1 &= -\frac{1}{l_r}\left[\frac{8\nu l_r}{(3-4\nu)k_r}+2\Xi'_{01}(k_r)-\frac{6\Xi'_{02}(k_r)}{(3-4\nu)^2}\right] \\ &\quad +\frac{2}{k_r}\left[-\Xi'_{11}(k_r)+\Xi'_{12}(k_r)\right] \\ f_2 &= -\frac{1}{l_r}\left[\frac{8\nu l_r}{(3-4\nu)k_r}-\frac{8\nu\Xi'_{02}(k_r)}{(3-4\nu)^2}\right]-\frac{2}{k_r}\left[-\Xi'_{11}(k_r)+\Xi'_{12}(k_r)\right] \\ \Xi'_{\hat{m}\hat{s}}(k_r) &= \begin{cases}\frac{\pi}{2}\left[H_0\left(\frac{b_{\hat{s}}k_r}{2l_r}\right)-Y_0\left(\frac{b_{\hat{s}}k_r}{2l_r}\right)\right](\hat{m}=0)\\ \frac{2l_r}{b_{\hat{s}}k_r}+1-\frac{\pi}{2}\left[H_1\left(\frac{b_{\hat{s}}k_r}{2l_r}\right)-Y_1\left(\frac{b_{\hat{s}}k_r}{2l_r}\right)\right](\hat{m}=1)\end{cases} \\ k_r &= \sqrt{(r'+1)^2+(t'+1)^2-2(r'+1)(t'+1)\cos\theta} \\ \cos\alpha &= \left[(r'+1)-(t'+1)\cos\theta\right]/k_r \end{aligned} \tag{27}$$

The stress and displacement fields at the surface in the model of an elastic half space subjected to an axisymmetric but non-uniform pressure on the surface are finally obtained, which are given in Eqs. (25)–(27).

4. Solutions of three typically axisymmetric contact problems

Based on the above general solutions, three typical problems are analyzed in this section, i.e., the Boussinesq model, contact model between a rigid flat-ended cylindrical indenter and an elastic half space as well as contact model between a rigid spherical indenter and an elastic half space.

4.1. An elastic half space under an axisymmetrically uniform pressure

As shown in Fig. 5, a uniform pressure is applied on an elastic half space in a circular region, i.e., $p(r)=p_0(r\le a)$. Using Eqs. (25)–(27) leads to closed-form solutions of the stress and displacement fields at the surface of the elastic half space,

$$\begin{cases} \bar{\sigma}_r = \frac{p_0}{16\pi l_r}\int_{-1}^1\int_0^{2\pi}\left[(f_1+f_2)+(f_1-f_2)\left(2\cos^2\alpha-1\right)\right] \\ \quad \left(t'+1\right)d\theta dt' \\ \bar{\sigma}_\theta = \frac{p_0}{16\pi l_r}\int_{-1}^1\int_0^{2\pi}\left[(f_2+f_1)+(f_2-f_1)\left(2\cos^2\alpha-1\right)\right] \\ \quad \left(t'+1\right)d\theta dt' \\ \bar{\sigma}_z = -\frac{p_0}{8\pi l_r^2}\int_{-1}^1\int_0^{2\pi}\left[\frac{8(1-\nu)l_r}{(3-4\nu)k_r}-2\Xi'_{01}(k_r)-\frac{2\Xi'_{02}(k_r)}{(3-4\nu)^2}\right] \\ \quad \left(t'+1\right)d\theta dt' \\ \bar{\tau}_{rz} = -\frac{p_0}{8\pi l_r^2}\int_{-1}^1\int_0^{2\pi}\left[\frac{4(1-2\nu)l_r}{(3-4\nu)k_r}-2\Xi'_{11}(k_r)+\frac{2\Xi'_{12}(k_r)}{(3-4\nu)^2}\right] \\ \quad \cos\alpha\left(t'+1\right)d\theta dt' \end{cases} \tag{28}$$

and

$$\begin{cases} \bar{u}_r = -\frac{p_0 a}{16\pi\mu l_r}\int_{-1}^1\int_0^{2\pi}\left[-\Xi'_{11}(k_r)+\Xi'_{12}(k_r)\right]\cos\alpha\left(t'+1\right)d\theta dt' \\ \bar{u}_z = \frac{p_0 a}{16\mu\pi l_r}\int_{-1}^1\int_0^{2\pi}\left[\Xi'_{01}(k_r)+\Xi'_{02}(k_r)\right]\left(t'+1\right)d\theta dt' \end{cases} \tag{29}$$

4.2. Contact model of a rigid flat-ended cylindrical indenter indenting an elastic half space

The frictionless contact between a rigid flat-ended cylindrical indenter of radius R and an elastic half space as shown in Fig. 6 is considered, where P is a resultant force in the z-direction, δ denotes the indent depth and the contact radius is $a=R$. The displacement at the surface of the elastic half space in the z-axis direction satisfies

$$\bar{u}_z=\delta=\text{const},\ (r\le a) \tag{30}$$

Substituting the second equation of Eq. (26) into Eq. (30) and then differentiating the resulting equation with respect to r yields

$$\frac{1}{\pi}\int_{-1}^1\frac{\text{kern}\left(r',t'\right)}{\sqrt{1-t'^2}}p\left[\frac{a}{2}\left(t'+1\right)\right]dt'=0 \tag{31}$$

where

$$\begin{aligned} \text{kern}\left(r',t'\right) &= \sqrt{1-t'^2}\int_0^{2\pi}\left(t'+1\right) \\ &\quad \cos\alpha\left[\begin{array}{l}\frac{2b_1}{\pi}-b_1H_1\left(\frac{b_1k_r}{2l_r}\right)+b_1Y_1\left(\frac{b_1k_r}{2l_r}\right)\\ +\frac{2b_2}{\pi}-b_2H_1\left(\frac{b_2k_r}{2l_r}\right)+b_2Y_1\left(\frac{b_2k_r}{2l_r}\right)\end{array}\right]d\theta \end{aligned} \tag{32}$$

In addition, the resultant force P should equal to the integral of $p(r)$ in the circular contact region, which leads to

$$\frac{1}{\pi}\int_{-1}^{1}(t'+1)p\left[\frac{a}{2}(t'+1)\right]dt' = \frac{2P}{\pi^2 a^2} \tag{33}$$

When the external load P and contact radius a are given, the contact pressure $p(r)$ could be determined by solving Eqs. (31) and (33). Compared with the solution of pressure in the classical contact model $p(r) = P/(2\pi a^2)/\sqrt{1-(r/a)^2}$, an analytical expression of the contact pressure considering surface effect is not easily achieved. Numerical solutions can be obtained by transforming Eqs. (31) and (33) into linear algebraic equations based on the numerical method proposed by Erdogan and Gupta (1972),

$$\mathbf{Bp} = \mathbf{f} \tag{34}$$

in which

$$\mathbf{B} = \left[\begin{bmatrix} b_{\hat{i}\hat{j}} \\ b_{\hat{n}\hat{j}} \end{bmatrix}\right], b_{\hat{i}\hat{j}} = \frac{1}{\hat{n}}\mathrm{kern}(r'_{\hat{i}}, t'_{\hat{j}}), b_{\hat{n}\hat{j}} = \frac{1}{\hat{n}}(t'_{\hat{j}}+1)\sqrt{1-t_{\hat{j}}'^2}$$

$$\mathbf{p} = \left[p'\left[(t'_1+1)a/2\right], p'\left[(t'_2+1)a/2\right], \cdots, p'\left[(t'_{\hat{n}}+1)a/2\right]\right]^{\mathrm{T}}$$

$$\mathbf{f} = \left[0, 0, \cdots, 0, 2P/(\pi^2 a^2)\right]^{\mathrm{T}}$$

$$\mathrm{kern}(r'_{\hat{i}}, t'_{\hat{j}}) = \sqrt{1-t_{\hat{j}}'^2}\int_0^{2\pi}(t'_{\hat{j}}+1)(\cos\alpha)_{\hat{i}\hat{j}} \times \begin{bmatrix} \frac{2b_1}{\pi} - b_1 H_1\left(\frac{b_1 k_r^{\hat{i}\hat{j}}}{2l_r}\right) + b_1 Y_1\left(\frac{b_1 k_r^{\hat{i}\hat{j}}}{2l_r}\right) \\ +\frac{2b_2}{\pi} - b_2 H_1\left(\frac{b_2 k_r^{\hat{i}\hat{j}}}{2l_r}\right) + b_2 Y_1\left(\frac{b_2 k_r^{\hat{i}\hat{j}}}{2l_r}\right) \end{bmatrix} d\theta$$

$$k_r^{\hat{i}\hat{j}} = \sqrt{(r'_{\hat{i}}+1)^2 + (t'_{\hat{j}}+1)^2 - 2(r'_{\hat{i}}+1)(t'_{\hat{j}}+1)\cos\theta}$$

$$(\cos\alpha)_{\hat{i}\hat{j}} = \left[(r'_{\hat{i}}+1) - (t'_{\hat{j}}+1)\cos\theta\right]/k_r^{\hat{i}\hat{j}}$$

$$r'_{\hat{i}} = \cos\left(\frac{\hat{i}}{\hat{n}}\pi\right)\left(\hat{i}=1,\cdots,\hat{n}-1\right),$$

$$t'_{\hat{j}} = \cos\left(\frac{2\hat{j}-1}{2\hat{n}}\pi\right)\left(\hat{j}=1,\cdots,\hat{n}\right) \tag{35}$$

Then, substituting the numerical solution of the contact pressure $p(r)$ into Eqs. (25) and (26) leads to the stress and displacement fields at the contact surface ($z=0$).

4.3. Contact model of a rigid spherical indenter indenting an elastic half space

As for the frictionless contact between a rigid spherical indenter of radius R and an elastic half space as shown in Fig. 7, a resultant force P in the z-direction acts on the spherical indenter, resulting in a circular contact region of radius a. In the classical contact model without considering surface effect, the contact radius can be expressed as $a_c = [3(1-\nu)PR/(8\mu)]^{1/3}$ and the pressure in the contact region can be formulated as $p(r) = 3P\sqrt{1-(r/a_c)^2}/(2\pi a_c^2)$ (Johnson, 1987), both of which would no longer be valid for a nano-scaled contact model with surface effect (Gao et al., 2013; Zhou and Gao, 2013). The vertical displacement at the surface of the elastic half space can be written as,

$$\bar{u}_z = \delta - \frac{r^2}{2R},\ (r \le a) \tag{36}$$

Substituting the second equation of Eq. (26) into Eq. (36) and then differentiating the resulting equation with respect to r leads to

$$\frac{\pi}{32\mu l_r^2}\frac{1}{\pi}\int_{-1}^{1}\frac{\mathrm{kern}(r',t')}{\sqrt{1-t'^2}}p\left[\frac{a}{2}(t'+1)\right]dt' = -\frac{a}{2R}(r'+1) \tag{37}$$

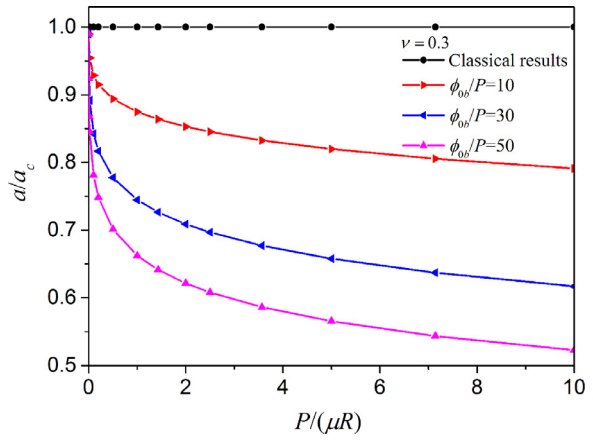

Fig. 11. The normalized contact radius a/a_c as a function of the dimensionless parameter $P/(\mu R)$ in the model of a rigid spherical indenter indenting an elastic half space for cases of different values of ϕ_{0b}/P.

In addition, Eq. (33) still holds in this model for the relationship between the resultant force P and the contact pressure $p(r)$ in the circular contact region.

Similarly, Eqs. (33) and (37) can be transformed to linear algebraic equations using the numerical method given by Erdogan and Gupta (1972),

$$\mathbf{Bp} = \mathbf{f}, \mathbf{B} = \left[\begin{bmatrix} b_{\hat{i}\hat{j}} \\ b_{\hat{n}\hat{j}} \end{bmatrix}\right], b_{\hat{i}\hat{j}} = \frac{1}{\hat{n}}\mathrm{kern}(r'_{\hat{i}}, t'_{\hat{j}}), b_{\hat{n}\hat{j}} = \frac{1}{\hat{n}}(t'_{\hat{j}}+1)\sqrt{1-t_{\hat{j}}'^2}$$

$$\mathbf{p} = \left[p'\left[(t'_1+1)a/2\right], p'\left[(t'_2+1)a/2\right], \cdots, p'\left[(t'_{\hat{n}}+1)a/2\right]\right]^{\mathrm{T}},$$

$$\mathbf{f} = \left[-\frac{16\mu a l_r^2}{\pi R}(r'_1+1), \cdots, -\frac{16\mu a l_r^2}{\pi R}(r'_{\hat{i}}+1), \cdots, -\frac{16\mu a l_r^2}{\pi R}(r'_{\hat{n}-1}+1), \frac{2P}{\pi^2 a^2}\right]^{\mathrm{T}}$$

$$\mathrm{kern}(r'_{\hat{i}}, t'_{\hat{j}}) = \sqrt{1-t_{\hat{j}}'^2}\int_0^{2\pi}(t'_{\hat{j}}+1)(\cos\alpha)_{\hat{i}\hat{j}} \times \begin{bmatrix} \frac{2b_1}{\pi} - b_1 H_1\left(\frac{b_1 k_r^{\hat{i}\hat{j}}}{2l_r}\right) + b_1 Y_1\left(\frac{b_1 k_r^{\hat{i}\hat{j}}}{2l_r}\right) \\ +\frac{2b_2}{\pi} - b_2 H_1\left(\frac{b_2 k_r^{\hat{i}\hat{j}}}{2l_r}\right) + b_2 Y_1\left(\frac{b_2 k_r^{\hat{i}\hat{j}}}{2l_r}\right) \end{bmatrix} d\theta$$

$$k_r^{\hat{i}\hat{j}} = \sqrt{(r'_{\hat{i}}+1)^2 + (t'_{\hat{j}}+1)^2 - 2(r'_{\hat{i}}+1)(t'_{\hat{j}}+1)\cos\theta}$$

$$(\cos\alpha)_{\hat{i}\hat{j}} = \left[(r'_{\hat{i}}+1) - (t'_{\hat{j}}+1)\cos\theta\right]/k_r^{\hat{i}\hat{j}}$$

$$r'_{\hat{i}} = \cos\left(\frac{\hat{i}}{\hat{n}}\pi\right)\left(\hat{i}=1,\cdots,\hat{n}-1\right), t'_{\hat{j}} = \cos\left(\frac{2\hat{j}-1}{2\hat{n}}\pi\right)\left(\hat{j}=1,\cdots,\hat{n}\right) \tag{38}$$

With regard to the above equations, the contact pressure $p(r)$ and the contact radius a can be solved numerically by a trial method, which has also been adopted by Long and Wang (2013). In order to find the real value, firstly, let the contact radius a equal a trial value a' (for example, a' can be taken as the classical value of contact radius $a_c = [3(1-\nu)PR/(8\mu)]^{1/3}$), then substitute a' into Eq. (38) to calculate the pressure $p(r)$. An abrupt drop or rise of the $p(r)$ curve near the contact edge indicates that a' is larger or smaller than the real value of a. Let a' decrease or increase a small value and start a new trial. The trial process would be finished when the slope of $p(r)$ curve near the contact edge satisfies the condition $|[(p'_1-p'_2)/(t'_1-t'_2)]^{[\tilde{m}]} - [(p'_2-p'_3)/(t'_2-t'_3)]^{[\tilde{m}]}|/|[(p'_2-p'_3)/(t'_2-t'_3)]^{[\tilde{m}]}| \le 0.05$ and the difference of the contact radii in the neighboring trials satisfies $|a'^{[\tilde{m}]} - a'^{[\tilde{m}-1]}|/a_c \le 0.001$, where $p'_{\tilde{j}} = p'[(t'_{\tilde{j}}+1)a/2]$, $(\tilde{j}=1,2,3)$ and $\tilde{m}$ denotes the trial number. Based on these two criteria, real solutions of the contact radius and the pressure can be found simultaneously.

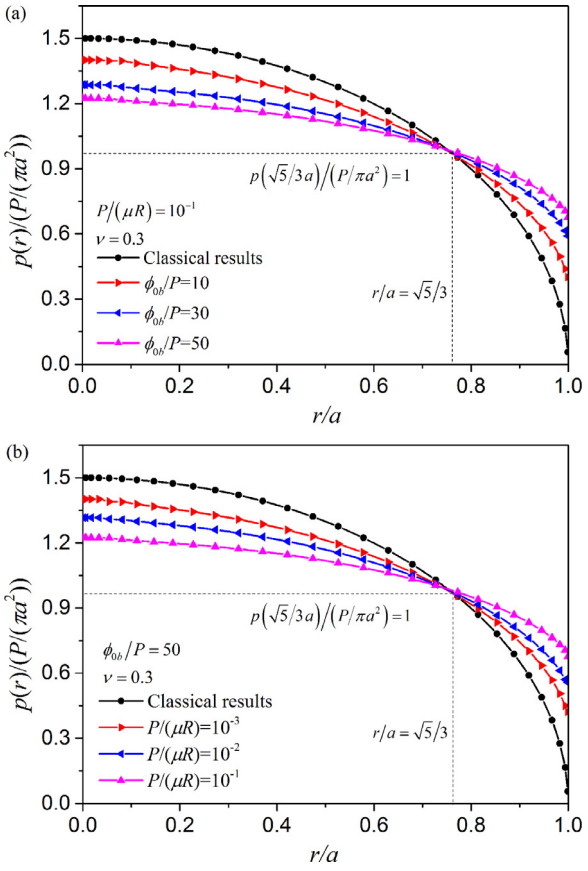

Fig. 12. Distribution of the non-dimensional contact pressure in the contact region of a rigid spherical indenter indenting an elastic half space. (a) For cases of different values of ϕ_{0b}/P; (b) For cases of different values of $P/(\mu R)$.

5. Results and discussion

Distributions of the stress and displacement fields at the surface of the elastic half space in three different kinds of models are analyzed and compared with the corresponding solutions in the classical contact mechanics without surface effect (Johnson, 1987). In the present paper, the Poisson's ratio of the elastic half space is taken as $\nu = 0.3$.

5.1. The case of an elastic half space under an axisymmetrically uniform pressure

Closed-form solutions of the stress and displacement fields at the surface of the elastic half space have been given in Eqs. (28) and (29) for the model of an elastic half space subjected to an axisymmetrically uniform pressure. Distributions of each stress and displacement component at the pressured surface are shown in Fig. 8. The corresponding counterparts in the classical Boussinesq model are also given for comparison.

It is clearly found that surface effect characterized by the dimensionless parameter $l_r = \phi_{0b}/(\mu a)$ on the stress fields at the surface of the elastic half space is much obvious. The radial, circumferential and normal stresses with a non-zero l_r deviate significantly from the classical counterparts as shown in Fig. 8(a)–(c), respectively. The surface effect leads to smoother stress distribution at the surface, which should be more reasonable than the discontinuous jump of the classical solutions at the loading edge $r = a$. Furthermore, in the loading area $r \leq a$, absolute values of all the stress components are remarkably smaller than the classical counterparts and the larger the dimensionless parameter l_r, the smaller the absolute value of all the stress components is. Outside the loading area $r > a$, the radial stress at the surface is much smaller than the classical tension stress, which even becomes a compressive one for a relatively large l_r as shown in Fig. 8(a). However, surface effect shows hardly influence on the circumferential stress outside the loading area as shown in Fig. 8(b). The vanishing normal stress outside the loading area in the classical solution becomes negative when the surface effect is considered. Furthermore, the larger the dimensionless parameter l_r, the larger the absolute value of the compressive normal stress is, which can be found in Fig. 8(c). Especially, the tangential stress in the classical model (Johnson, 1987) does not vanish anymore and achieves the maximum at the loading edge, which is due to the non-zero surface-induced tangential traction (tangential traction induced by surface effect) as shown in Fig. 8(d).

Both the radial and normal displacements become smaller than their classical counterparts as shown in Fig. 8(e) and (f), which further demonstrates a fact that the nano-scaled contact area as well as its vicinity is stiffened due to surface effect. It can be concluded that all the stress and displacement components depend significantly on surface effect when the dimensionless parameter l_r related to the bulk surface energy density of the indented material is non-vanishing. All the results would approach the classical ones when the surface effect becomes weak.

5.2. The case of a rigid flat-ended cylindrical indenter indenting an elastic half space

Similar to the above Boussinesq model, the dimensionless parameter l_r, as an important factor characterizing surface effect in nano-contact problems, affects significantly the contact behavior of a rigid flat-ended cylindrical indenter indenting an elastic half space.

Distribution of contact pressure between a rigid flat-ended cylindrical indenter and an elastic half space is plotted in Fig. 9 for different values of dimensionless parameter l_r, where the classical result is also given for comparison. It is found that due to the surface-induced normal traction, the contact pressure $p(r)$ is obviously smaller and more uniform than the classical one (Johnson, 1987). Besides, the singularity still exists at the contact edge of the rigid flat-ended cylindrical indenter. Similar results are also found in Pinyochotiwong et al. (2013) based on the G-M model. When the surface effect becomes significant, i.e., an increasing l_r, deviation between the contact pressure with surface effect and the classical one becomes larger and larger. Furthermore, it demonstrates that the classical closed-form solution of the contact pressure cannot be adopted approximately to describe that in the model considering surface effect.

Distributions of the normal and shear stresses as well as the normal displacement at the surface $z = 0$ are illustrated in Fig. 10(a)–(c), respectively. It can be easily found that the absolute value of the compressive normal stress with surface effect is smaller than the classical one in the contact area as shown in Fig. 10(a), while additional non-zero compressive stress exists outside the contact area induced by the surface effect, different from the traction free condition in the classical model. Another interesting phenomenon is that in contrast to a vanishing shear stress at the surface in the classical solution, a non-zero one exists in spite of the frictionless assumption as shown in Fig. 10(b), which is due to the additional surface-induced tangential traction given in the second equation of Eq. (11). As shown in Fig. 10(c), the normal displacement with surface effect decreases with an increasing dimensionless parameter l_r, which indicates reasonably a hardening result induced by surface effect. Moreover, in the contact area, the normal displacement always keeps a constant regardless of whether the surface effect is considered or not, which satisfies

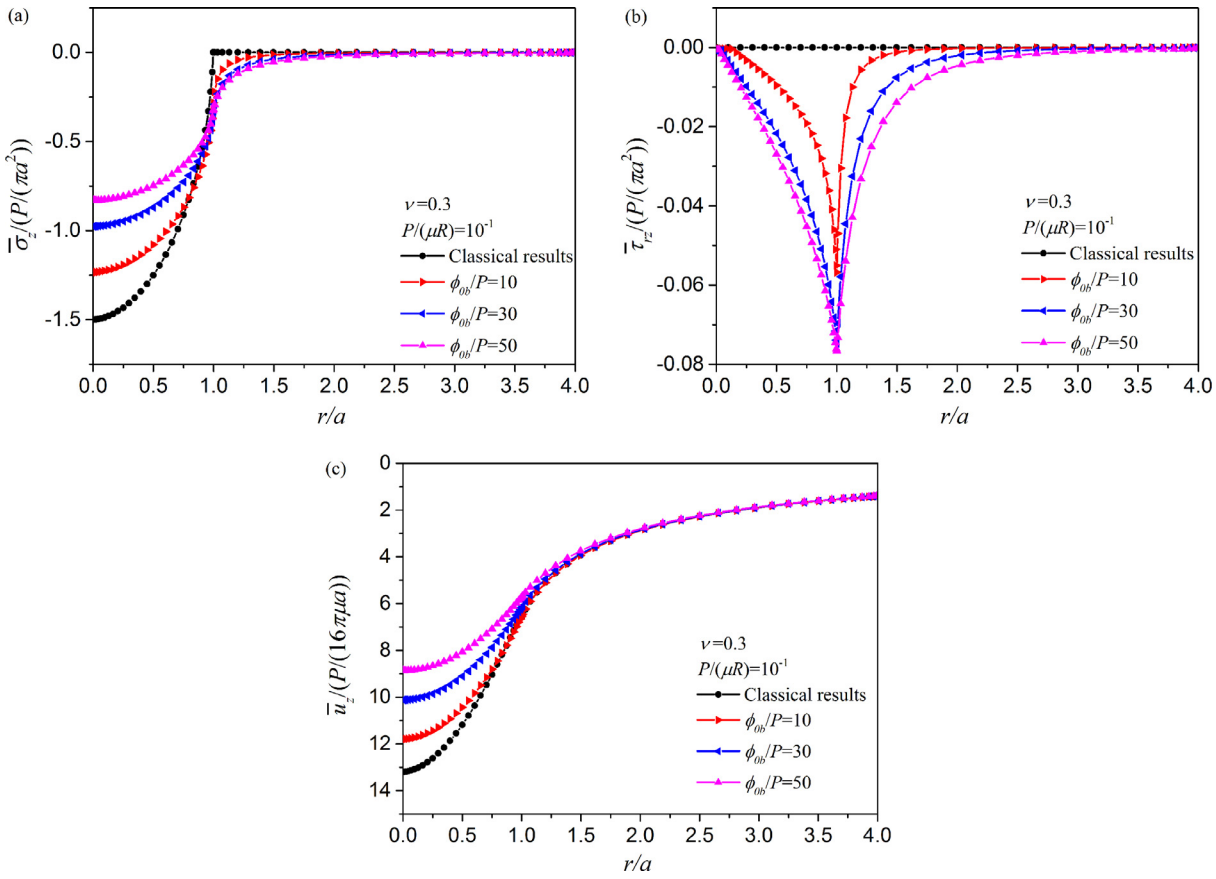

Fig. 13. The effect of bulk surface energy density of the indented material on the stress and displacement at the contact surface in the model of a rigid spherical indenter indenting an elastic half space. (a) For the non-dimensional normal stress $\bar{\sigma}_z$; (b) For the non-dimensional shear stress $\bar{\tau}_{rz}$; (c) For the non-dimensional normal displacement $\bar{u}_z$.

the boundary condition between the rigid flat-ended cylindrical indenter and the elastic half space.

5.3. The case of a rigid spherical indenter indenting an elastic half space

Different from the above two cases, both the contact radius a and the contact pressure $p(r)$ are unknown in the model of a rigid spherical indenter indenting an elastic half space, which should be simultaneously determined with a preset external force P. Scaling analysis shows that two dimensionless parameters are introduced in the present model, i.e., ϕ_{0b}/P characterizing the surface effect and $P/(\mu R)$ representing the size effect of indenter radius.

The relation between the contact radius normalized by the classical one a/a_c and the normalized external loading $P/(\mu R)$ is shown in Fig. 11 for different ϕ_{0b}/P. It is clear to see that the contact radius with surface effect is much smaller than the classical one. For a given value of ϕ_{0b}/P, the parameter a/a_c decreases with an increasing $P/(\mu R)$ indicating that the smaller the indenter radius or the bulk shear modulus, the larger the deviation between the classical contact radius and the one with surface effect will be. When the indenter radius or the bulk shear modulus increases, i.e., a decreasing parameter $P/(\mu R)$, a/a_c approaches to 1, demonstrating that the surface effect could be neglected in cases with an indenter of relatively large radius or a harder substrate. For a determined value of $P/(\mu R)$, parameter a/a_c decreases with an increasing ϕ_{0b}/P, which means the larger the bulk surface energy density of the indented material, the smaller the contact radius is. In a word, surface effect makes the indented material hardened.

Distribution of the contact pressure $p(r)$ in the contact area normalized by the average pressure $P/(\pi a^2)$ is plotted in Fig. 12(a) and (b) for fixed parameters $P/(\mu R)$ and ϕ_{0b}/P, respectively. It is found that either an increasing bulk surface energy density in the case with a given $P/(\mu R)$ or a decreasing indenter radius or bulk shear modulus in the case with a fixed ϕ_{0b}/P, would enhance surface effect, leading to a more uniform distribution of the present result than the classical prediction. Since there exists the relation $p(r)/[P/(\pi a^2)] = 1.5\sqrt{1-(r/a)^2}$ in classical contact mechanics (Johnson, 1987), it can be solved that the contact pressure would equal to the average one at $r/a = \sqrt{5}/3$. It is interesting to find that all the contact pressures in different cases would intersect at the point of $r/a \approx 0.745$, inside which the present contact pressure would decrease and approach to the average pressure, while beyond which it would increase and approach to the average one, along with the increase of surface effect, as shown in Fig. 12(a) and (b). Furthermore, the contact pressure does not vanish at the contact edge $r = a$ any more due to a non-zero surface-induced normal traction.

Distributions of the normal and tangential stresses as well as the normal displacement at the contact surface are given in Figs. 13(a)–(c) and 14(a)–(c) for fixed parameters $P/(\mu R)$ and ϕ_{0b}/P, respectively. Similar to the above two models, not only an increasing bulk surface energy density but also a decreasing indenter radius or bulk shear modulus should enhance surface effect on the contact behaviors, which yield a more uniformly distributed normal stress, a non-zero tangential one and a smaller normal displacement as compared with the classical predictions. An interesting phenomenon is that the shear stress at contact sur-

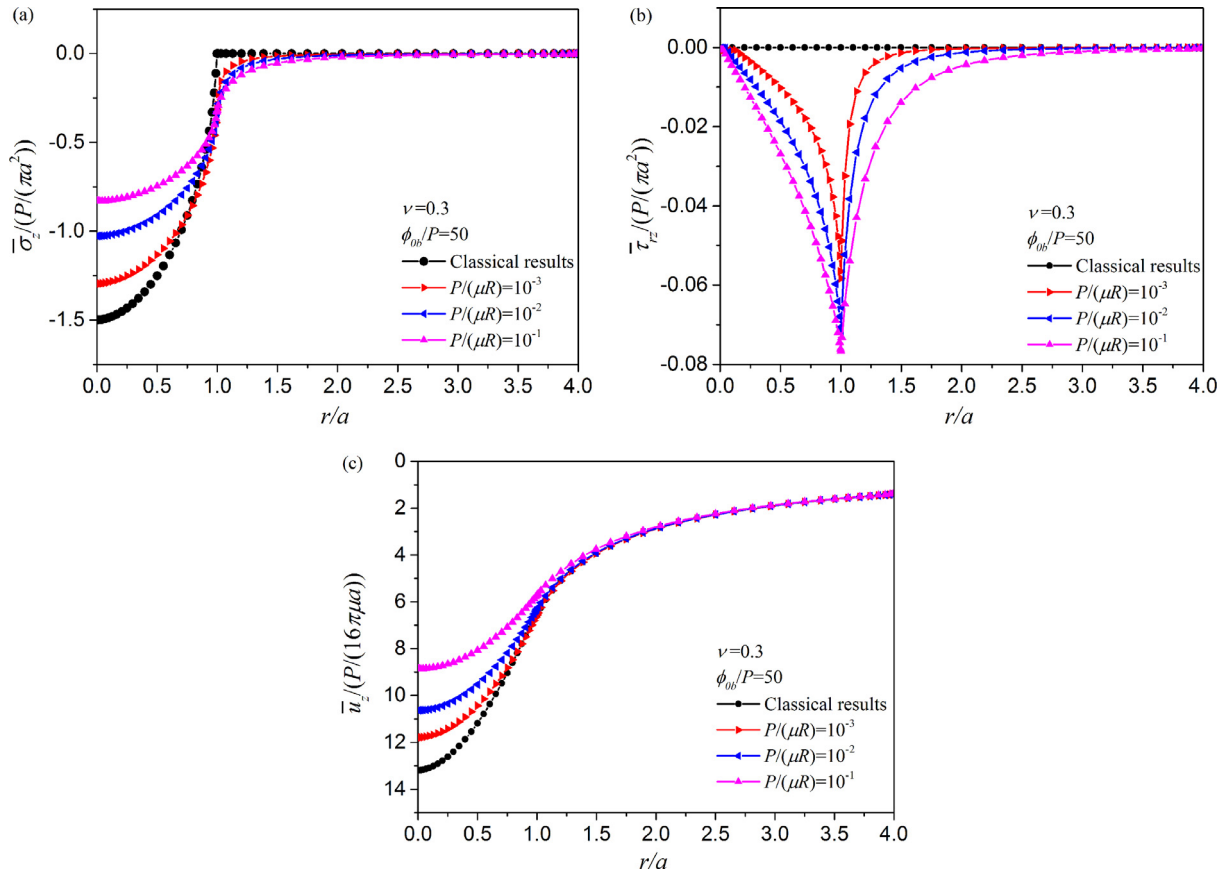

Fig. 14. Effects of radius of the spherical indenter and the bulk shear modulus on the stress and displacement at the contact surface in the model of a rigid spherical indenter indenting an elastic half space. (a) For the non-dimensional normal stress $\bar{\sigma}_z$; (b) For the non-dimensional shear stress $\bar{\tau}_{rz}$; (c) For the non-dimensional normal displacement $\bar{u}_z$.

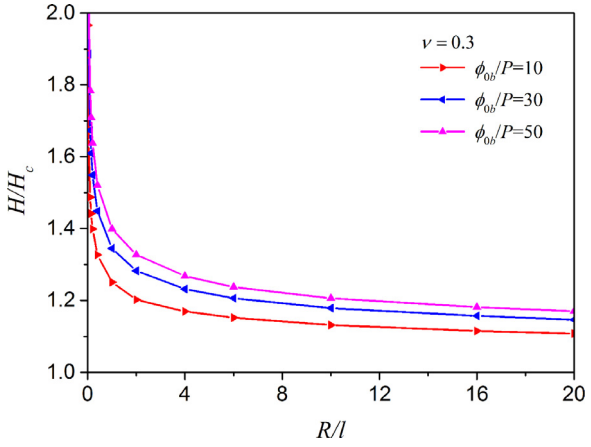

Fig. 15. Normalized nano-indentation hardness H/H_c as a function of the dimensionless parameter R/l in the model of a rigid spherical indenter indenting an elastic half space for cases of different values of ϕ_{0b}/P.

face becomes non-zero even though the friction between the rigid indenter and half-space is neglected, which is different from the zero-shear stress predicted by Long and Wang (2013). The deviation is due to the tangential component of the surface-induced traction in the boundary condition, as shown in Eq. (11), which was not included in Long and Wang (2013) only considering the effect of a surface tension.

Surface effect on the nano-indentation hardness is further investigated with the model of a rigid spherical indenter indenting an elastic half space. The nano-indentation hardness predicted by the present model is defined as $H = P/(\pi a^2)$ and that yielded by the classical contact model is $H_c = P\pi^{-1}[3(1-\nu)PR/(8\mu)]^{-2/3}$ (Johnson, 1987). The normalized nano-indentation by the classical one as a function of the dimensionless radius of the spherical indenter R/l is shown in Fig. 15 for cases with different ϕ_{0b}/P. It is found that the indentation hardness with surface effect is obviously larger than the classical one and increases with the decease of indenter radius. When the parameter R/l and bulk surface energy density ϕ_{0b} are determined, it is found that the smaller the external force P, the larger the predicted nano-indentation hardness will be.

6. Conclusions

To characterize the surface effect in nano-contact behaviors, three axisymmetric contact models are established and analyzed using an elastic theory for nanomaterials based on surface energy density, including an elastic half space subjected to a uniformly normal pressure, the frictionless contact between an elastic half space and a rigid flat-ended cylindrical indenter as well as the frictionless contact between an elastic half space and a spherical indenter. The Love's strain function method and Hankel integral transformation are adopted to obtain the general solution of the stress and displacement fields at the surface of an elastic half space subjected to an arbitrarily but axisymmetrically distributed pressure. An intrinsic length characterizing surface effect is found, which equals to the ratio of the bulk surface energy density to the bulk shear modulus. Based on the general solution, surface effect on the stresses and displacements at the contact surface in

the three kinds of models are analyzed. When the contact radius is on the same order as the intrinsic length, surface effect on the elastic fields and contact behaviors is very obvious, which cannot be predicted by the classical contact model. It is found that surface effect could be strengthened not only by increasing the bulk surface energy density of the indented material but also by decreasing the bulk shear modulus or the indenter size (contact radius). Compared with the classical solutions, surface effect leads to much smoother and more uniformly distributed normal stresses and a smaller vertical displacement at the contact surface. A special phenomenon is that in comparison with the classical prediction, a non-zero shear stress exists at the contact surface in spite of the frictionless assumption. The nano-indentation hardness is further discussed based on the spherical indenter model. It is found that surface effect would show significant influence on the nano-indentation hardness, which could be enhanced with the decrease of the indenter radius or the external force. The results in this paper should be helpful not only for deep understanding of surface effect in nano-contact behaviors but also for further revealing the nature of size-dependent nano-indentation hardness.

Acknowledgments

The work reported here is supported by NSFC through Grants (no. 11532013, no. 11372317, no. 11402270), the BIT Creative Research Plan, the Project of Beijing Municipal Science and Technology Commission (no. Z161100001416007) and the Project of State Key Laboratory of Explosion Science and Technology (no. ZDKT17-02).

References

Abramowitz, M., Stegun, I.A., 1964. Handbook of Mathematical Functions: With Formulas, Graphs, and Mathematical Tables. Courier Corporation.
Cammarata, R.C., 1994. Surface and interface stress effects in thin films. Prog. Surf. Sci. 46, 1–38.
Chan, C.K., Peng, H., Liu, G., Mcilwrath, K., Zhang, X.F., Huggins, R.A., Cui, Y., 2007. High-performance lithium battery anodes using silicon nanowires. Nat. Nanotechnol 3, 187–191.
Chen, S.H., Yao, Y., 2014. Elastic theory of nanomaterials based on surface-energy density. J. Appl. Mech. 81, 121002.
Chen, W., Zhang, C., 2010. Anti-plane shear Green's functions for an isotropic elastic half-space with a material surface. Int. J. Solids Struct. 47, 1641–1650.
Chhapadia, P., Mohammadi, P., Sharma, P., 2011. Curvature-dependent surface energy and implications for nanostructures. J. Mech. Phys. Solids 59, 2103–2115.
Cuenot, S., Frétigny, C., Demoustier-Champagne, S., Nysten, B., 2004. Surface tension effect on the mechanical properties of nanomaterials measured by atomic force microscopy. Phys. Rev. B 69, 165410.
Dingreville, R., Qu, J., 2008. Interfacial excess energy, excess stress and excess strain in elastic solids: planar interfaces. J. Mech. Phys. Solids 56, 1944–1954.
Dingreville, R., Qu, J., Cherkaoui, M., 2005. Surface free energy and its effect on the elastic behavior of nano-sized particles, wires and films. J. Mech. Phys. Solids 53, 1827–1854.
Duan, H.L., Wang, J., Huang, Z.P., Karihaloo, B.L., 2005. Size-dependent effective elastic constants of solids containing nano-inhomogeneities with interface stress. J. Mech. Phys. Solids 53, 1574–1596.
Erdogan, F., Gupta, G., 1972. On the numerical solution of singular integral equations(Singular integral equations numerical solution from Gauss-Chebyshev formulas for mixed boundary value problems). Q. Appl. Math. 29, 525–534.
Gao, X., Hao, F., Fang, D., Huang, Z., 2013. Boussinesq problem with the surface effect and its application to contact mechanics at the nanoscale. Int. J. Solids Struct. 50, 2620–2630.
Gao, X., Huang, Z., Fang, D., 2017. Curvature-dependent interfacial energy and its effects on the elastic properties of nanomaterials. Int. J. Solids Struct. 113, 100–107.
Gao, X., Huang, Z., Qu, J., Fang, D., 2014. A curvature-dependent interfacial energy-based interface stress theory and its applications to nano-structured materials: (I) General theory. J. Mech. Phys. Solids 66, 59–77.
Gerberich, W., Tymiak, N., Grunlan, J., Horstemeyer, M., Baskes, M., 2002. Interpretations of indentation size effects. J. Appl. Mech. 69, 433–442.
Gerberich, W.W., Kramer, D.E., Tymiak, N.I., Volinsky, A.A., Bahr, D.F., Kriese, M.D., 1999. Nanoindentation-induced defect–interface interactions: phenomena, methods and limitations. Acta Mater. 47, 4115–4123.
Gibbs, J.W., 1906. The Scientific Papers of J. Willard Gibbs. Green and Company, Longmans.
Gurtin, M.E., Murdoch, A.I., 1975. A continuum theory of elastic material surfaces. Arch. Ration. Mech. Anal. 57, 291–323.
Gurtin, M.E., Murdoch, A.I., 1978. Surface stress in solids. Int. J. Solids Struct. 14, 431–440.
Hajji, M., 1978. Indentation of a membrane on an elastic half space. J. Appl. Mech. 45, 320–324.
He, J., Lilley, C.M., 2008. Surface stress effect on bending resonance of nanowires with different boundary conditions. Appl. Phys. Lett. 93, 263108.
He, L., Lim, C., 2006. Surface Green function for a soft elastic half-space: influence of surface stress. Int. J. Solids Struct. 43, 132–143.
He, L., Lim, C., Wu, B., 2004. A continuum model for size-dependent deformation of elastic films of nano-scale thickness. Int. J. Solids Struct. 41, 847–857.
Huang, Z., 2010. Erratum to: size-dependent effective properties of a heterogeneous material with interface energy effect: from finite deformation theory to infinitesimal strain analysis. Acta Mech. 215, 363–364.
Huang, Z., Sun, L., 2007. Size-dependent effective properties of a heterogeneous material with interface energy effect: from finite deformation theory to infinitesimal strain analysis. Acta Mech. 190, 151–163.
Huang, Z., Wang, J., 2006. A theory of hyperelasticity of multi-phase media with surface/interface energy effect. Acta Mech. 182, 195–210.
Huang, Z., Wang, J., 2010. Erratum to: a theory of hyperelasticity of multi-phase media with surface/interface energy effect. Acta Mech. 215, 365–366.
Huang, Z.P., Wang, J.X., 2013. Micromechanics of nanocomposites with interface energy effect. Handbook of Micromechanics and Nanomechanics. Pan Stanford Publishing.
Jia, N., Yao, Y., Yang, Y., Chen, S., 2017a. Analysis of two-dimensional contact problems considering surface effect. Int. J. Solids Struct 125, 172–183.
Jia, N., Yao, Y., Yang, Y., Chen, S., 2017b. Size effect in the bending of a Timoshenko nanobeam. Acta Mech. 228, 2363–2375.
Jia, N., Yao, Y., Yang, Y., Chen, S., 2017c. Surface effect on the resonant frequency of Timoshenko nanobeams. Int. J. Mech. Sci. 133, 21–27.
Jing, G.Y., Duan, H.L., Sun, X.M., Zhang, Z.S., Xu, J., Li, Y.D., Wang, J.X., Yu, D.P., 2006. Surface effects on elastic properties of silver nanowires: contact atomic-force microscopy. Phys. Rev. B 73, 235409.
Johnson, K.L., 1987. Contact Mechanics. Cambridge university press.
Koguchi, H., 2008. Surface Green function with surface stresses and surface elasticity using Stroh's formalism. J. Appl. Mech. 75, 061014.
Long, J., Wang, G., 2013. Effects of surface tension on axisymmetric Hertzian contact problem. Mech. Mater. 56, 65–70.
Long, J., Wang, G., Feng, X., Yu, S., 2012. Two-dimensional Hertzian contact problem with surface tension. Int. J. Solids Struct. 49, 1588–1594.
Mi, C., Jun, S., Kouris, D.A., Kim, S.Y., 2008. Atomistic calculations of interface elastic properties in noncoherent metallic bilayers. Phys. Rev. B 77, 439–446.
Miller, R.E., Shenoy, V.B., 2000. Size-dependent elastic properties of nanosized structural elements. Nanotechnology 11, 139.
Nguyen, T.B., Rungamornrat, J., Senjuntichai, T., 2016. Analysis of planar cracks in 3D elastic media with consideration of surface elasticity. Int. J. Fract. 202, 51–77.
Nguyen, T.B., Rungamornrat, J., Senjuntichai, T., Wijeyewickrema, A.C., 2015. FEM-S-GBEM coupling for modeling of mode-I planar cracks in three-dimensional elastic media with residual surface tension effects. Eng. Anal. Boundary Elem. 55, 40–51.
Nix, W.D., Gao, H.J., 1998. An atomistic interpretation of interface stress. Scr. Mater. 39, 1653–1661.
Pinyochotiwong, Y., Rungamornrat, J., Senjuntichai, T., 2013. Rigid frictionless indentation on elastic half space with influence of surface stresses. Int. J. Eng. Sci. 71, 15–35.
Poncharal, P., Wang, Z., Ugarte, D., De Heer, W.A., 1999. Electrostatic deflections and electromechanical resonances of carbon nanotubes. Science 283, 1513–1516.
Qi, W., Wang, M., 2004. Size and shape dependent melting temperature of metallic nanoparticles. Mater. Chem. Phys. 88, 280–284.
Rogers, J.A., Someya, T., Huang, Y., 2010. Materials and mechanics for stretchable electronics. Science 327, 1603–1607.
Rungamornrat, J., Tuttipongsawat, P., Senjuntichai, T., 2016. Elastic layer under axisymmetric surface loads and influence of surface stresses. Appl. Math. Model 40, 1532–1553.
Selvadurai, A.P., 2000. Partial Differential Equations in Mechanics 2: The Biharmonic Equation, Poisson's Equation. Springer Science & Business Media.
Sharma, P., Ganti, S., Bhate, N., 2003. Effect of surfaces on the size-dependent elastic state of nano-inhomogeneities. Appl. Phys. Lett. 82, 535–537.
Shenoy, V.B., 2005. Atomistic calculations of elastic properties of metallic fcc crystal surfaces. Phys. Rev. B 71, 094104.
Shuttleworth, R., 1950. The surface tension of solids. Proc. Phys. Soc. London, Sect. A 63, 444.
Steigmann, D., Ogden, R., 1997. Plane deformations of elastic solids with intrinsic boundary elasticity. In: Proceedings of the Royal Society of London. Series A: Mathematical, Physical and Engineering Sciences, 453, pp. 853–877.
Steigmann, D., Ogden, R., 1999. Elastic surface—substrate interactions. Proc. R. Soc. London. Ser. A 455, 437–474.
Streitz, F.H., Cammarata, R.C., Sieradzki, K., 1994. Surface-stress effects on elastic properties. I. Thin metal films. Phys. Rev. B 49, 10699–10706.
Takrori, F.M., Ayyad, A., 2017. Surface energy of metal alloy nanoparticles. Appl. Surf. Sci. 401, 65–68.
Timoshenko, S., Goodier, J., 1951. Theory of Elasticity. McGraw Hill, New York.
Tirapat, S., Senjuntichai, T., Rungamornrat, J., 2017. Influence of surface energy effects on elastic fields of a layered elastic medium under surface loading. Adv. Mater. Sci. Eng. 2017, 1–11.

Vasu, T.S., Bhandakkar, T.K., 2016. A study of the contact of an elastic layer–substrate system indented by a long rigid cylinder incorporating surface effects. J. Appl. Mech. 83, 061009.
Wang, G., Feng, X., 2007a. Effects of surface stresses on contact problems at nanoscale. J. Appl. Phys. 101, 013510.
Wang, G.F., Feng, X.Q., 2007b. Effects of surface elasticity and residual surface tension on the natural frequency of microbeams. Appl. Phys. Lett. 90, 231904.
Wei, Y., Wang, X., Zhao, M., 2004. Size effect measurement and characterization in nanoindentation test. J. Mater. Res. 19, 208–217.
Wolfer, W.G., 2011. Elastic properties of surfaces on nanoparticles. Acta Mater. 59, 7736–7743.
Yao, Y., Chen, S., 2016a. Buckling behavior of nanowires predicted by a new surface energy density model. Acta Mech. 227, 1799–1811.
Yao, Y., Chen, S., Fang, D., 2017. An interface energy density-based theory considering the coherent interface effect in nanomaterials. J. Mech. Phys. Solids 99, 321–337.
Yao, Y., Chen, S.H., 2015. Surface effect on resonant properties of nanowires predicted by an elastic theory for nanomaterials. J. Appl. Phys. 118, 044303.
Yao, Y., Chen, S.H., 2016b. Surface effect in the bending of nanowires. Mech. Mater. 100, 12–21.
Yao, Y., Wei, Y., Chen, S., 2015. Size effect of the surface energy density of nanoparticles. Surf. Sci. 636, 19–24.
Zhang, C., Yao, Y., Chen, S., 2014. Size-dependent surface energy density of typically fcc metallic nanomaterials. Comput. Mater. Sci. 82, 372–377.
Zhang, T.-Y., Xu, W.-H., 2002. Surface effects on nanoindentation. J. Mater. Res. 17, 1715–1720.
Zhang, W., Wang, T., Chen, X., 2010. Effect of surface/interface stress on the plastic deformation of nanoporous materials and nanocomposites. Int. J. Plast. 26, 957–975.
Zhao, X., Rajapakse, R., 2009. Analytical solutions for a surface-loaded isotropic elastic layer with surface energy effects. Int. J. Eng Sci 47, 1433–1444.
Zhou, S.-S., Gao, X.-L., 2014. Solutions of the generalized half-plane and half-space Cerruti problems with surface effects. Z. Angew. Math. Phys. 66, 1125–1142.
Zhou, S., Gao, X.-L., 2013. Solutions of half-space and half-plane contact problems based on surface elasticity. Z. Angew. Math. Phys. 64, 145–166.